THE JOURNAL OF PHYSICAL CHEMISTRY B

ARTICLE

pubs.acs.org/JPCB

Reorganization Energy for Internal Electron Transfer in Multicopper Oxidases

LiHong Hu,[†,‡] Maryam Farrokhnia,[†,§] Jimmy Heimdal,[†] Sergey Shleev,[∥] Lubomír Rulíšek,[⊥] and Ulf Ryde*[,†]

[†]Department of Theoretical Chemistry, Lund University, Chemical Centre, P.O. Box 124, SE-221 00 Lund, Sweden

[‡]School of Computer Science and Information Technology, Northeast Normal University, Changchun 130117, People's Republic of China

[§]The Persian Gulf Marine Biotechnology Research Center, Bushehr University of Medical Sciences, Bushehr, Iran

[∥]Biomedical Laboratory Science and Technology, Faculty of Health and Society, Malmö University, SE-205 06 Malmö, Sweden

[⊥]Institute of Organic Chemistry and Biochemistry, Gilead Sciences Research Center at IOCB, Academy of Sciences of the Czech Republic, Flemingovo náměstí 2, 166 10 Praha 6, Czech Republic

Supporting Information

ABSTRACT: We have calculated the reorganization energy for the intramolecular electron transfer between the reduced type 1 copper site and the peroxy intermediate of the trinuclear cluster in the multicopper oxidase CueO. The calculations are performed at the combined quantum mechanics and molecular mechanics (QM/MM) level, based on molecular dynamics simulations with tailored potentials for the two copper sites. We obtain a reorganization energy of 91−133 kJ/mol, depending on the theoretical treatment. The two Cu sites contribute by 12 and 22 kJ/mol to this energy, whereas the solvent contribution is 34 kJ/mol. The rest comes from the protein, involving small contributions from many residues. We have also estimated the energy difference between the two electron-transfer states and show that the reduction of the peroxy intermediate is exergonic by 43−87 kJ/mol, depending on the theoretical method. Both the solvent and the protein contribute to this energy difference, especially charged residues close to the two Cu sites. We compare these estimates with energies obtained from QM/MM optimizations and QM calculations in a vacuum and discuss differences between the results obtained at various levels of theory.

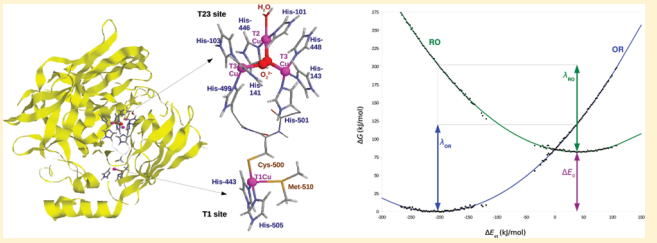

INTRODUCTION

The transfer of electrons between sites in the same or different proteins is a very important process in biochemistry and therefore has attracted much interest.[1,2] Marcus theory provides a powerful theoretical framework for electron transfer.[3] It estimates the rate of nonadiabatic electron transfer by the equation:

$$k_{et} = |H_{DA}|^2 \frac{\hbar}{\sqrt{4\pi\lambda kT}} \exp\left(-\frac{(\Delta G + \lambda)^2}{4\lambda kT}\right) \quad (1)$$

where ΔG is the driving force of the reaction (i.e., the difference in the redox potential), H_{DA} is the electronic coupling between the donor and the acceptor, and λ is the reorganization energy (RE). The RE is the energy required to relax the structure and environment upon electron transfer, that is, the energy difference of the product state in its equilibrium geometry and in the equilibrium geometry of the reactant state, and vice versa.

Experiments can provide accurate values for driving force and rate constants. However, it is usually difficult to obtain direct and quantitative estimates for the RE from experiment.[1,4] Rather few experimentally determined estimates have been reported, for example, for intraprotein electron transfer in Ru-modified azurin and cytochromes, the primary charge separation in the bacterial photosynthetic reaction center, and the interprotein electron transfer between two cytochromes.[5−10] The results indicate that the RE is 25−90 kJ/mol if the cofactors are excluded from the solvent and 90−150 kJ/mol if the cofactors are solvent exposed.[10]

Many theoretical methods have been developed to estimate REs. The RE is often divided into two parts, the inner-sphere RE, which comes from the redox site itself, and the outer-sphere RE, which comes from the surrounding protein and solvent. The inner-sphere RE can be estimated by quantum mechanical (QM) methods from the definition of the RE, that is, by calculating the energy difference between the oxidized state in its equilibrium geometry, $E^{ox}_{QM}(R_{ox})$, and in the equilibrium geometry of the reduced state, $E^{ox}_{QM}(R_{red})$, and vice versa, using small models of the redox-active site in the calculations (e.g., a metal ion and its first-sphere ligands):[11−13]

$$\lambda_{is} = E^{ox}_{QM}(R_{red}) - E^{ox}_{QM}(R_{ox}) \quad (2)$$

For a protein site, it is more accurate to use combined QM and molecular-mechanics (QM/MM) methods to obtain the structures

Received: June 23, 2011
Revised: September 23, 2011
Published: September 28, 2011

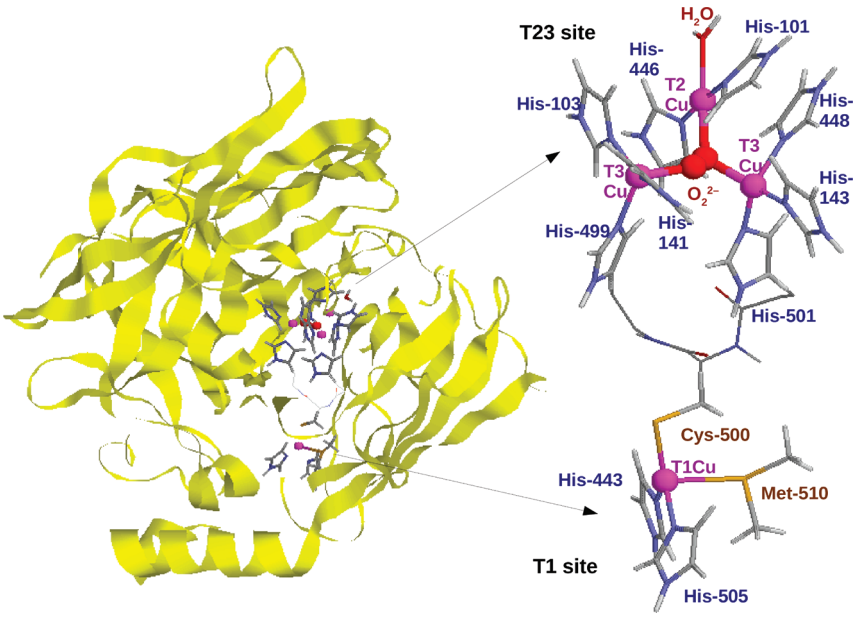

Figure 1. The general structure of CueO (left) and a detailed structure of the two copper centers (right), including the backbone linkage between the two His T23 Cu ligands and the Cys T1 ligand.

of the redox site, and it is typically observed that the inner-sphere RE is lower when calculated in the protein than in a vacuum.[12,14,15]

However, estimating the outer-sphere RE requires more complicated methods, normally based on molecular-dynamics (MD) simulations of a fully solvated protein. A common approach, originally suggested by Warshel,[16] is based on Marcus parabolas and a linear-response approximation. It has been used in several studies.[16−25] Several other groups have developed extensions to this theory, as well as other methods to calculate the RE at various levels of theory, including MM, QM/MM, and QM.[20,21,23,26] In particular, it has been shown that the RE in a protein can be estimated from QM or QM/MM calculations on snapshots from classical MD simulations.[15,27] Similar methods have also been used to estimate redox potentials of cofactors in proteins.[15,28]

The multicopper oxidases (MCOs) are a large group of proteins that catalyze the oxidation of various organic and inorganic compounds with the concomitant reduction of O_2 to H_2O.[29,30] The group includes laccase, ascorbate oxidase, ceruloplasmin, bilirubin oxidase, CueO, and Fet3p. The MCOs contain at least two redox-active copper sites, a mononuclear type 1 (blue) copper site (T1), close to the surface of the protein, where substrates bind and are oxidized, and a trinuclear type 2 and 3 copper cluster (T23), where O_2 is reduced (Figure 1). The T1 Cu ion is coordinated to one Cys, two His, and often a Met residue. The three T23 Cu ions are ligated by eight His residues and a number (1−3, depending on the state of the enzyme) of ligands derived from H_2O and O_2. The two sites are ∼13 Å apart, and they are connected by the protein backbone between the Cys ligand of the T1 site and two neighboring His residues, which are both ligands of two copper ions in the T23 cluster.[29,31,32]

Recently, it has been suggested that the reaction mechanism of the MCOs involves an uphill intramolecular electron-transfer (IET) step.[33−35] Many biological systems contain an uphill electron-transfer step, and it has been hypothesized that this feature exists to avoid the need of optimizing individual rates.[36] This suggestion can be justified by correlating observed differences in redox potentials and IET rates. However, for this, an estimate of the RE is needed. Therefore, we here calculate the total RE of a MCO using an approach similar to that developed by Warshel, Sprik, and Blumberger:[15,16,20] We run classical MD simulations of a solvated MCO, using tailored accurate MM parametrizations of the two metal sites, and then perform QM/MM calculations of the individual metal sites for over a thousand snapshots from the MD simulations. We apply several different QM/MM approaches to obtain inner- and outer-sphere RE, as well as residue and solvent components to the RE. We also compare the results to those obtained with minimized QM or QM/MM structures. As a byproduct, we also obtain estimates of the free-energy difference of the two electron-transfer states.

METHODS

The Protein. The calculations on the MCOs are based on the 1.4 Å crystal structure of CueO (PDB code 1KV7; Figure 1).[32] CueO is a bacterial copper homeostasis factor, and this structure was selected because of its high resolution and that this protein lacks the extended glycosylation found for most eukaryotic MCOs. In addition, we have already performed extensive theoretical studies on this protein.[37−41] The whole protein was included in the calculations, as well as a varying amount of solvent water molecules (see below). All Glu and Asp residues were assumed to be deprotonated, and all Lys and Arg residues were assumed to be protonated. The protonation state of the His residues was assigned on the basis of their solvent exposure, the hydrogen-bond network, and the local surroundings:[37] Eight His residues on the protein surface were assumed to be protonated on both N atoms (His-145, 224, 314, 405, 406, 465, 488, and 494), whereas the remaining 10 His residues, which are ligands of the T1 and T23 Cu ions, were assumed to be protonated on the N atom not coordinating to the metal. The Cys ligand of the T1 Cu site was assumed to be deprotonated.

Two states of each of the two copper sites were considered. The T1 site was either in the reduced (Cu^I) or the oxidized (Cu^{II}) states. For the T23 site, we considered either the peroxy

intermediate (PI; $Cu^{I}Cu^{II}{}_2O_2{}^{2-}H_2O$), with $O_2{}^{2-}$ in the center of the cluster and a water ligand coordinated to the type 2 copper ion, or the corresponding one-electron reduced state, which is a variant of the native intermediate before the cleavage of the O−O bond (NI′).[37] The former state was combined with a reduced state of the T1 site (called the RO state) and the latter state was combined with the oxidized state of the T1 site (called the OR state), so that we studied the electron transfer between the reduced T1 site and T23 cluster in the PI state. This gave a net charge of the full simulated system of +1 in both states. No counterions were used in the simulations.

MD Simulations. All MD simulations were carried out with the sander module in the Amber 10 software,[42] using the Amber 1999 force field.[43,44] The bond lengths involving hydrogen atoms were constrained using the SHAKE algorithm.[45] The electrostatics were treated using the particle-mesh Ewald method[46,47] with a grid size of 80^3, a fourth-order B-spline interpolation, a tolerance of 10^{-5}, and a real-space cutoff of 8 Å. The temperature was kept constant at 300 K using the Berendsen weak-coupling algorithm[48] with a time constant of 1 ps, and the pressure was kept constant at 1 atm with a time constant of 1 ps. The MD time step was 2 fs, and the nonbonded pair list was updated every 50 fs.

Five simulations were run. First, the structures were subjected to 1000 steps minimization, keeping all non-hydrogen atoms restrained to the original crystal structure with a force constant of 418 kJ/mol/Å^2. Next, a 20 ps MD simulation with a constant volume was run, still keeping the heavy atoms restrained. Third, a 20 + 50 ps MD simulation with a constant pressure was run to equilibrate the box size. During the first 20 ps, the non-hydrogen atoms were restrained, whereas during the last 50 ps, these restraints were removed. Fourth, a 200 ps equilibration at a constant volume was run without any restraints. Finally, the systems were simulated for 10 ns in a constant volume, and coordinates were sampled every 2 ps. MD simulations were performed for both electronic states, RO and OR. The MD simulations were performed with explicit water molecules (12 270 water molecules in both states), using the TIP3P water model.[49]

QM Calculations. QM calculations were performed with the Perdew−Burke−Ernzerhof (PBE) density functional[50] and the def2-SVP basis set.[51] These calculations were sped up by expanding the Coulomb interactions in an auxiliary basis set, the resolution-of-identity (RI) approximation.[52,53] Vibrational frequencies were calculated at the same level of theory. Zero-point and thermal corrections to the Gibbs free energy (at 300 K and 1 atm pressure) were calculated from these frequencies using a normal-mode, harmonic-oscillator, ideal-gas approximation.[54] Test calculations were also performed with the hybrid B3LYP method[55,56] and with the larger def2-TZVP basis set.[51] All QM calculations were performed with the Turbomole software.[57] We used a $Cu(imidazole)_2(CH_3S)(CH_3SCH_3)$ model for the T1 site and a $Cu_3(imidazole)_8(H_2O)(O_2)$ model for the T23 cluster. The two QM systems were studied in both the oxidized and the reduced states. This means that the T1 site had a total charge of either zero or one, with no or one unpaired electron. The T23 cluster had a total charge of either +3 or +2 and two or one unpaired electrons. The unrestricted formalism was used for all calculations, except for the reduced state of the T1 site. For the oxidized state of the T23 cluster (the PI), it was assumed that the two unpaired electrons are antiferromagnetically coupled, in accordance with experiments (i.e., giving an open-shell singlet).[58] Continuum-solvation free energies were estimated with the COSMO model in Turbomole, using the default optimized radii (and 2.0 Å for Cu).[59−61]

The QM/MM-2QM Approach. QM studies of internal electron transfer in proteins are not trivial. If both redox-active sites are included in one QM calculations, a single electronic state is obtained, whereas the other state (after electron transfer) will be an excited state that is hard to converge and characterize. Therefore, we have used a QM/MM approach in which the two sites are treated in separate QM calculations. This approach also avoids the self-interaction problems with DFT.[15] Such an approach is applicable only if the two redox sites are spatially separated, which is the case in CueO, where the T1 and T23 copper centers are ∼13 Å apart. Theoretically, this approach is a simple extrapolation of the standard QM/MM approach to two separate QM systems. Technically, it requires new programs. The QM/MM-2QM implementation is based on the ComQum approach,[14,62] which is an interface between the Turbomole and Amber softwares.[42,57]

In this QM/MM-2QM approach, the protein and solvent are divided into three subsystems: the two QM systems (systems 1a and 1b) and the MM system (system 2). In the QM calculations, systems 1a and 1b are represented by a wave function, whereas all of the other atoms are represented by an array of partial point charges, one for each atom, taken from MM libraries. Thereby, the polarization of the QM system by the surroundings is included in a self-consistent manner (electrostatic embedding, EE).

In some calculations (called protein fixed), the MM system was kept fixed at the original (crystallographic) coordinates. Such calculations were run to ensure that the surroundings reside in the same local minimum in all calculations, making the energies stable, although all outer-sphere reorganization is ignored. In other calculations (called protein free), all residues and solvent molecules within 6 Å of the two QM systems were allowed to relax by a full MM minimization in each cycle of the QM optimization.

When there is a bond between systems 1 (1a or 1b) and 2 (a junction), the hydrogen link-atom approach is employed: The QM region is truncated by hydrogen atoms (called hydrogen link atoms, HL), the positions of which are linearly related to the corresponding carbon atoms in the full system (called carbon link atoms, CL).[62,63] In the point-charge model of the surroundings, all atoms were included, except the CL atoms.[64,66] The two QM systems were the same as in the vacuum QM calculations. Therefore, the CB atom of all His and Met Cu ligands, and the CA atom of the Cys ligand were replaced by HL atoms.

The total QM/MM energy is calculated in the following way:

$$E^{\mathrm{EE}}_{\mathrm{QM/MM\text{-}2QM}} = E^{\mathrm{HL}}_{\mathrm{QM1a\,+\,ptch1b2}} - E^{\mathrm{HL}}_{\mathrm{MM1a},\,q=0} + E^{\mathrm{HL}}_{\mathrm{QM1b\,+\,ptch1a2}} - E^{\mathrm{HL}}_{\mathrm{MM1b},\,q=0} + E^{\mathrm{CL}}_{\mathrm{MM1ab2},\,q_{1a}=q_{1b}=0} \quad (3)$$

Here, $E^{\mathrm{HL}}_{\mathrm{QM1a+ptch1b2}}$ is the QM energy of system 1a, truncated with HL atoms, and including a point-charge model of the surrounding protein in the one-electron Hamiltonian (also of system 1b). $E^{\mathrm{HL}}_{\mathrm{QM1b+ptch1a2}}$ is the corresponding QM energy for system 1b. $E^{\mathrm{HL}}_{\mathrm{MM1a},q\,=\,0}$ is the MM energy of system 1a (still with HL atoms), but with all charges zeroed, and similar for $E^{\mathrm{HL}}_{\mathrm{MM1b},q\,=\,0}$. Finally, $E^{\mathrm{CL}}_{\mathrm{MM1ab2},q_{1a}=q_{1b}=0}$ is the MM energy of the full system with CL atoms, but with the charges of the two QM systems zeroed (because all electrostatics interactions within the QM systems and between the QM and MM systems are considered in the two QM terms). However, the electrostatic interactions between the two QM systems are still accounted for in both $E^{\mathrm{HL}}_{\mathrm{QM1a+ptch1a2}}$ and $E^{\mathrm{HL}}_{\mathrm{QM1b+ptch1a2}}$. This problem was solved by scaling down the point charges of the

other QM system by a factor of 2 in both terms. This is not completely satisfactory, because it will underestimate the polarization of the QM systems by each other, but because the two systems are quite far apart, the effect should be quite small.

The point-charge model of each QM system was obtained by a fit to the electrostatic potential (ESP) calculated for a polarized wave function but without the point charges when the ESP was calculated. The ESP points were sampled with the Merz–Kollman approach,[65] as implemented in Turbomole.[57] The charges were updated in each step of the geometry optimization. The same charges were used to model the QM systems at the MM level when the surrounding MM system was optimized.

This EE approach was used for all QM/MM-2QM geometry optimizations. For the calculations of the redox potential and the reorganization energy, we also tested to calculate the energies with mechanical embedding (ME). This means that the QM systems are not polarized by the MM system. Instead, the QM/MM-2QM energy was calculated according to:

$$E^{\mathrm{ME}}_{\mathrm{QM/MM\text{-}2QM}} = E^{\mathrm{HL}}_{\mathrm{QM1a}} - E^{\mathrm{CL}}_{\mathrm{MM1a}} + E^{\mathrm{HL}}_{\mathrm{QM1b}} - E^{\mathrm{CL}}_{\mathrm{MM1b}} + E^{\mathrm{CL}}_{\mathrm{MM1ab2}} \quad (4)$$

Here, $E^{\mathrm{HL}}_{\mathrm{QM1a}}$ and $E^{\mathrm{HL}}_{\mathrm{QM1b}}$ are the QM energy of the two QM systems, truncated with HL atoms, but without any point-charge model. $E^{\mathrm{CL}}_{\mathrm{MM1a}}$ and $E^{\mathrm{CL}}_{\mathrm{MM1a}}$ are the corresponding MM energies of the two QM systems, but now with CL atoms and with full charges. Finally, $E^{\mathrm{CL}}_{\mathrm{MM1ab2}}$ is the MM energy of the total system with CL atoms and full charges.

The advantage with the ME approach is that the electrostatic interactions are calculated at the MM level with correct charges and positions of the CL atoms, whereas in the EE approach, electrostatic interactions between the QM and MM systems are calculated with HL atoms at slightly different positions and with a charge density characteristic for a HL atom, rather than the real CL atoms.[64] Moreover, in the ME approach, the electrostatic interactions are pairwise decomposable, making it easier to interpret the results. In the ME approach, the inner- and outer-sphere REs are also separable. Therefore, ME is our default method to calculate the energies. On the other hand, EE allows the QM systems to be polarized by each other and by the MM system (but this leads to a problem with double-counting, as we saw above; this problem is avoided by ME). EE is normally considered to be preferable,[66] although it will lead to unbalanced calculations (the QM systems are polarized by the MM systems, but the MM system is not polarized), which leads to problems with overpolarization of the QM system.[64,67] In our ME approach, we used ESP charges from a polarized wave function, so that polarization of the QM system is included in the charge model.

A final problem with the EE energies is that the point-charge model of one QM system depends on the ESP charges from the other QM system so that the calculations should strictly be run in an iterative manner until the ESP charges and the QM energy no longer changes. In the geometry optimization, this is no problem because the geometry optimization is already iterative and the changes in the geometry in the last step are so small that the ESP charges hardly change. However, for the calculation of the RE, it is a problem, because the change in the geometry is significant. In the single-point calculations of the REs from the QM/MM minimized structures, we solved this problem by calculating the energies iteratively, updating the ESP charges after each wave function calculation. On the other hand, for the EE calculations on the MD structures, no iterations were used.

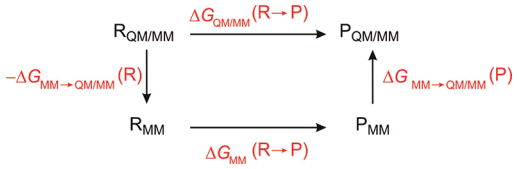

Figure 2. The QTCP thermodynamic cycle.[68,69]

The QM/MM-2QM calculations were performed on spherical systems in which the whole CueO protein was solvated in a 38 Å sphere of explicit water molecules.[37]

QTCP-2QM Calculations. For the QM/MM minimized structures, we also used the QTCP (QM/MM thermodynamic cycle perturbation) approach to calculate the redox potentials.[68,69] This is a method to calculate free energies with a high-level QM/MM method, using sampling only at the computationally cheaper MM level. It employs the thermodynamic cycle in Figure 2 and calculates the free energy from three separate terms:

$$\Delta G_{\mathrm{QTCP}}(\mathrm{R}\rightarrow\mathrm{P}) = -\Delta G_{\mathrm{MM}\rightarrow\mathrm{QM/MM}}(\mathrm{R}) + \Delta G_{\mathrm{MM}}(\mathrm{R}\rightarrow\mathrm{P}) + \Delta G_{\mathrm{MM}\rightarrow\mathrm{QM/MM}}(\mathrm{P}) \quad (5)$$

where R and P are the reactant and product states (in our case the OR and RO states). To obtain stable MM→QM/MM free energies, the QM systems need to be kept fixed in the MD simulations. Test calculations at the semiempirical level have shown that this does not affect the final free energies significantly.[70]

The QTCP calculations were performed as previously described,[68,69,71,72] with simple extensions to the QM/MM-2QM case: First, each redox state was optimized by QM/MM-2QM, using a solvated spherical system with a radius of 38 Å.[37] Second, the total system was moved into a periodic octahedral box and was further solvated with water molecules extending at least 9 Å from the original system, giving a total of 12 270 water molecules (a set of QTCP calculations in which the solvent shell was increased to 15 Å or 19 803 water molecules was also performed). For one state (we tested both the RO and the OR states), the system was first subjected to a 1000 step minimization, keeping the QM systems fixed and all heavy atoms except water molecules restrained toward their positions in the crystal structure with a force constant of 418 kJ/mol/Å^2. Next, two 20 ps MD simulations were run with the same heavy atoms still restrained. The first simulation was run with a constant volume, the second with a constant pressure. Finally, the box size was equilibrated by a 50 ps MD simulation with a constant pressure and with only the heavy atoms in the QM system restrained. The final structure of this simulation was then used as the starting structure for the simulations of the other state. It is not possible to keep the QM atoms exactly fixed in the constant-pressure simulations. Therefore, the QM atoms were moved back to the QM/MM structure before an equilibration of 200 ps and a production simulation of 400 ps were run with a constant volume and with the QM system fixed. During the production run, 200 snapshots were collected every 2 ps. Finally, free energies were estimated from these snapshots, using FEP or thermodynamic integration (TI). We used the method of statistical inefficiency and block averaging to ensure that the sampled data were independent (i.e., that the sampling time was longer than the correlation time).[73,74] FEP free energies and their uncertainties were estimated by cumulant expressions.[73]

The perturbations were divided into several steps: We performed nine simulations with the geometry of the reactant state,

but with charges of the QM system that were linearly transformed from the reactant state to the product state by a coupling parameter, λ, assuming the values of 0, 0.125, 0.25, 0.375, 0.5, 0.625, 0.75, 0.875, and 1. This was accomplished by simply changing the charges in the parameter file, whereas the coordinates of the QM system were kept to those of the reactant state. Free energies were estimated by TI. Next, the coordinates of the QM system were perturbed from that of the reactant state to that of the product state, using charges of the product state. This was accomplished in five FEP simulations using another coupling parameter attaining the values of 0, 0.25, 0.5, 0.75, and 1. For the two end states (reactant and product states), we also performed a perturbation from MM to QM/MM-2QM energies, as has been detailed before[69] with simple extensions to the 2QM case. The EE approach was employed. All calculations where automatized and performed by four Linux shell scripts and a number of Fortran programs that are available from the authors upon request. Some further details of the calculations can be found in http://www.teokem.lu.se/~ulf/Methods/qtcp.html.

QM/MM-PBSA-2QM Calculations. The QM/MM-PBSA method[75] can be viewed as a postprocessing of QM/MM calculations to obtain more stable energies, including a proper solvation energy by using continuum solvation methods. It is an adaptation of the widely used MM/PBSA approach[76] for QM/MM calculations. In this approach, an approximation to the total free energy for each state is obtained from:

$$G = E^{\mathrm{ME}}_{\mathrm{QM/MM-2QM}} + G_{\mathrm{solv}} + G_{\mathrm{np}} - TS_{\mathrm{QM/MM}} \qquad (6)$$

where $E^{\mathrm{ME}}_{\mathrm{QM/MM\text{-}2QM}}$ is the ME QM/MM-2QM energy in eq 4, and G_{Solv} is the polar solvation energy, estimated by a continuum approach, in our case obtained by solving the Poisson–Boltzmann (PB) equation using the PB solver in Amber.[42] G_{np} is the nonpolar solvation energy, estimated from the solvent-accessible surface area (SASA), through the linear relation G_{np} = 0.0227 SASA (Å^2) + 3.85 kJ/mol.[77] Finally, T is the temperature and $S_{\mathrm{QM/MM}}$ is the entropy, calculated from the frequencies, using a normal-mode harmonic-oscillator and ideal-gas approximation.[75] In this investigation, we assume that the contribution from the surrounding protein cancels between the reactant and the product, as has been done before,[72,75] so only the entropy of the isolated QM systems in vacuum was considered.

Several variants of QM/MM-PBSA are available.[75] In this Article, we used version 2 in ref 75, in which the electrostatic interaction energy between the QM and MM systems is calculated at the MM level, that is, with the ME approach. With two QM systems, it means that we use the $E^{\mathrm{ME}}_{\mathrm{QM/MM\text{-}2QM}}$ energy in eq 4. The QM energies and the ESP charges were calculated from vacuum wave functions. The QM/MM-PBSA-2QM calculations are based on the spherical QM/MM-2QM structures. The calculations were automatized and performed by Linux shell scripts, which are available from the authors on request. Further details of the calculations can be found in http://www.teokem.lu.se/~ulf/Methods/qmmm_pbsa.html.

Force-Field Parametrizations. The bonded force-field parameters of the copper sites in the MD simulations were constructed according to the method developed by Norrby and Liljefors,[78] using the recent implementation for Amber[79] (in the QM/MM-2QM minimizations, the internal MM energy of the two QM systems cancels, eqs 3 and 4; therefore, no bonds between the Cu ions and there ligands were defined). This method minimizes a penalty function consisting of the deviation of geometries and Hessian elements between the QM and MM calculations, giving different weights to different kinds of data. The geometries were described as lists of all bonds, angles, and dihedral angles, rather than by absolute positions. The weight factors of the various data types were 100 Å^{-1} for bonds, 2 deg^{-1} for angles, 1 deg^{-1} for torsions, and 0.01–0.1 mol Å^2/kcal for Hessian elements (0.01 for elements involving interactions of an atom with itself, 0.02 for atoms bound to each other, 0.04 for atoms connected by two bonds, 0.1 for atoms connected by three bonds, and 0.01 for all other elements).[78,80] The QM calculations were performed on the vacuum-optimized structures, which were started from the QM/MM-2QM structures in the protein.

The iterative force-field optimizations were started from the corresponding Hess2FF force field,[81] which is automatically extracted from the Hessian matrix. After convergence, the force field was checked. Typically, some bonds and angles get zero force constants in the first runs of the parametrizations. These were reset to reasonable values, and force constants of other angles around the same central atom were reduced, and then the parametrization was run again. This was repeated until all bonds and angles had nonzero force constants and all other parameters looked reasonable. Further instructions for the procedure are found in http://www.teokem.lu.se/~ulf/Methods/ponparm.html.

Specific force fields were calculated for both the reduced and the oxidized forms of the T1 and T23 centers. We assigned separate atom types for all metals and all atoms that ligated directly to the metals. For the T1 sites, we also used new atom types for all atoms in the ligands, except for hydrogen atoms bound to the same atom, whereas for the T23 site, we used standard Amber parameters for all atoms in the ligands, besides the one bound to the metal. All force-field parameters for the Cu sites are given in the Supporting Information.

Charges for all atoms were fitted to the ESP, sampled according to the Merz–Kollman scheme,[65] but with a higher-than-default density of points, 2000–3000 points/atom. These charges were used directly in the parametrization, whereas in the MD simulations of the whole protein, the charges on the CL atoms were adapted so that the total charge of the amino acid (including both QM and MM atoms) was the same as the sum of QM charges of the corresponding QM fragment.[14] Thereby, we ensure that the total charge of the simulated system is an integer, but we allow for charge transfer within the QM system (the amino acids with QM atoms have noninteger total charges). The van der Waals parameters of the Cu ions were R = 1.17 Å and ε = 4.77 kJ/mol.[82] Neither the charges nor the van der Waals parameters were changed during the parametrization.

Calculation of Reorganization Energies and Redox Potentials. The RE was calculated by three methods. For the minimized QM and QM/MM structures, we used the definition in eq 2, the energy difference between the oxidized state in its equilibrium geometry and in the geometry of the reduced state, and vice versa. For the MD simulations, we calculated the vertical energy difference between the two electronic states, RO and OR, $\Delta E_{\mathrm{et}} = E_{\mathrm{RO}} - E_{\mathrm{OR}}$ for all snapshots obtained in the MD simulations of the two states. Next, the RE was estimated from

$$\lambda = \frac{\langle \Delta E_{\mathrm{et}} \rangle_{\mathrm{RO}} - \langle \Delta E_{\mathrm{et}} \rangle_{\mathrm{OR}}}{2} \qquad (7)$$

where the brackets indicate averages over MD simulations, run either for the RO or for the OR states, as is specified by the subscripts.[15,20−22,27]

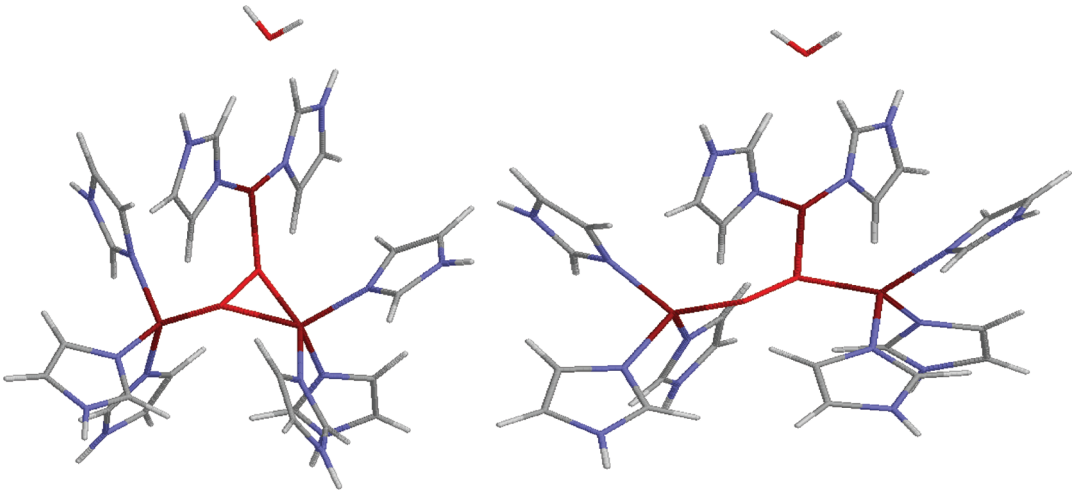

Figure 3. QM optimized structures of the PI (left) and NI′ (right) states.

Alternatively, ΔE_{et} was defined as the reaction coordinate and the free energy for each state was estimated from the probability of each energy ($p(\Delta E_{et})$, obtained by binning all of the calculated ΔE_{et} energy differences):[16−18]

$$\Delta G = RT \ln p(\Delta E_{et}) \quad (8)$$

The free-energy curves obtained from the two MD simulations were then fitted to harmonic functions, and the REs were estimated from the difference in energy on the fitted curves between the optimum ΔE_{et} for the RO and OR states.

The redox potentials of the two copper sites were also estimated. For the minimized QM and QM/MM-2QM structures, we used the relation:

$$E^0 = (E_{ox} - E_{red}) - E_{NHE} \quad (9)$$

where the factor E_{NHE} = 4.28 V converts the energy scale to that of the normal hydrogen electrode (NHE).[83] If both copper sites are considered, the correction factor cancels, and we give the energy difference between the OR and RO (a negative sign indicates that the OR state is more stable). For the MD simulations, we instead used the relation:[15,20−22,27]

$$E^0 = \frac{\langle \Delta E_{et} \rangle_{RO} + \langle \Delta E_{et} \rangle_{OR}}{2} \quad (10)$$

ΔE_{et} was calculated by the QM/MM-2QM approach, using either ME (eq 4) or EE (eq 3). The same charges of each Cu site were used in all calculations (both with EE and with ME). The reason for this is that previous investigations of the accuracy of QM/MM have indicated that the ESP charge fitting often becomes unstable and may give spurious charges and energies in some cases.[64] The calculations were performed on 1250 snapshots, sampled every 8 ps during the 10 ns production simulation. For the MM components, instead 5000 snapshots were used, sampled every 2 ps. In all calculations of ΔE_{et} with QM/MM-2QM or QTCP-2QM, no periodic boundary conditions were used. Instead, the MM system was centered on the two Cu sites, and an infinite cutoff was employed.

RESULTS AND DISCUSSION

In this study, we have calculated the RE for the internal electron transfer between the T1 and T23 centers in the MCO enzyme CueO (Figure 1). The MCOs catalyze the four-electron reduction of O_2 to H_2O in the T23 cluster, coupled to one-electron oxidation of various substrates in the T1 site. Therefore, the T1 site has only two oxidation states (Cu^I and Cu^{II}), whereas the T23 cluster has at least four different oxidation levels (formally Cu^I_3, $Cu^I_2Cu^{II}$, $Cu^ICu^{II}_2$, and Cu^{II}_3, although O_2 and H_2O in various oxidation levels are also involved).[29,37] Therefore, the reaction mechanism should involve four distinct steps of IET from the T1 site to the T23 cluster, which all may have different REs.

We have decided to study one of these steps, the reduction of the PI. This intermediate is formed by the binding of O_2 to the fully reduced (Cu^I_3) state of the protein. By a combination of experimental and theoretical studies, it is now widely accepted that it contains O_2 bound in a diagonal manner in the center of the T23 cluster (Figure 3a).[29,37−40,84,85] As the name indicates, O_2 is directly reduced upon binding by two electrons from two Cu^I ions so that the formal oxidation states of the T23 cluster are $Cu^ICu^{II}_2O_2^{2-}$. One-electron reduction of this complex, probably followed by a protonation, triggers the cleavage of the O−O bond and the formation of the native intermediate (NI), which contains a fully oxidized T23 site (Cu^{II}_3) with O^{2-} in the center and probably OH^- bridging the two T3 Cu ions.[29,37,38,40,41,86−88] The steps following the NI involve three reduction and protonation steps, leading to the release of two water molecules and the formation of the fully reduced state again, but for these intermediates, little experimental or structural information is available. Therefore, we have concentrated on the reduction of the PI in this study. We assume that the internal electron transfer is not coupled to the following protonation and O−O cleavage steps. Thus, we assume that there is a distinct short-lived intermediate that is at the formal $Cu^I_2Cu^{II}O_2^{2-}$ oxidation state, which we have called the NI′ state.[37,41] The structure can be obtained with QM or QM/MM methods, and it is shown in Figure 3b.[37] We also assume that ligand of the T2 Cu ion is water.

Redox Potentials of Minimized QM and QM/MM Structures. We started with calculations on minimized structures, obtained either for isolated QM systems in a vacuum (QM structures) or with QM/MM-2QM for the whole CueO protein. These calculations allow us to obtain both redox potentials and reorganization energy, albeit without any conformational sampling (thus, no free energies are obtained, meaning that strictly we obtain ionization energies rather than reduction potentials).

Table 1. Redox Potentials (V), Calculated by QM or QM/MM, the Latter with Either Mechanical (ME) or Electrostatic Embedding (EE) and with the Surroundings Either Fixed (fix) or Free to Relax[a]

	T1	T23	MM	total
QM, vac, PBE/B1	0.58	4.92		−4.34
QM, vac, PBE/B2//PBE/B1	0.79	5.09		−4.30
QM, vac, PBE/B2	0.80	5.10		−4.30
QM, vac, B3LYP/B1//PBE/B1	0.57	5.07		−4.50
QM, vac, B3LYP/B1	0.60	5.01		−4.41
QM, vac, B3LYP/B2//PBE/B1	0.78	5.39		−4.61
QM, vac, B3LYP/B2	0.83			
QM, ε = 4, PBE/B1	−0.20	1.40		−1.60
QM, ε = 80, PBE/B1	−0.52	−0.23		−0.29
ME, fix	0.37	4.55	3.42	−0.75
ME, free	0.39	4.70	3.21	−1.10
EE, fix, it1	−2.59	−2.22	−0.02	−0.39
EE, fix, it2	−2.56	−2.21	−0.02	−0.37
EE, fix, it3	−2.56	−2.21	−0.02	−0.37
EE, free, it1	−2.58	−2.96	−0.80	−0.42
EE, free, it2	−2.55	−2.95	−0.80	−0.40
EE, free, it3	−2.55	−2.95	−0.80	−0.40
QM/MM-PBSA, fix	0.37	4.55	3.01	−1.16
QM/MM-PBSA, free	0.39	4.70	3.06	−1.25
QTCP, RO simulation			3.79	−0.45
QTCP, OR simulation			3.74	−0.48
QTCP, RO simulation, more water[b]			3.74	−0.43
QTCP, OR simulation, more water[b]			3.77	−0.46

[a] The EE calculations are done iteratively because the ESP charges of one QM system affect the wavefunction of the other QM system. If nothing else is indicated, the calculations were performed with the PBE method and the def2-SVP basis set (denoted B1). For the vacuum calculations, we also tested the B3LYP method and the def2-TZVP basis set (denoted B2), in various combinations. If two methods are given, the first was used for the energy and the second was used for the geometry optimizations. Moreover, calculations in a COSMO continuum solvent with a dielectric constant of 4 or 80 were performed. The first two columns give redox potentials of the T1 and T23 centres, from the QM calculations. The MM column gives the net MM energy, and the last column gives the net QM/MM energy. For these two, a negative sign indicates that the OR state is most stable. To all QM energies have been added the zero-point energy and thermal corrections to the Gibbs free energy, obtained from a frequency calculation of the isolated QM systems at the PBE/B1 level (0.06 eV for the T1 site and 0.28 eV for the T23 Cu cluster). [b] Water solvation extending by 15 Å from the protein on all sides, instead of 9 Å.

The calculated redox potentials are presented in Table 1. The potential of the isolated T1 site varies from 0.58 V in a vacuum to −0.52 V in water-like continuum solvent. The potential does not change significantly if the functional is changed from PBE to B3LYP, but it increases by 0.2 V if the basis set is also increased to def2-TZVP. Single-point calculations give almost the same results as calculations with optimized structures, as is normally assumed. Experimentally, the redox potential of T1 sites with this set of ligand in various proteins is 0.3−0.7 V[33,35,89,90] (that of CueO is 0.4−0.5 V, depending on pH[91]), showing that only the estimates obtained in a low-dielectric medium are in a reasonable range.

The redox potential of the isolated T23 cluster is 4.9 V in a vacuum, but it changes to −0.23 V in a water-like continuum solvent. Thus, the calculations on the isolated clusters indicate that OR state (the NI and an oxidized T1 site) is more stable than the RO state, although in water the difference is only 28 kJ/mol. The potential of the T23 cluster increases by 0.15 V if the functional is changed to B3LYP and by a further 0.32 V if the basis set is also increased to def2-TZVP.

Table 2. Cu−Ligand Distances of the T1 Site Obtained in the QM and QM/MM-2QM Calculations with the Surrounding Fixed at the Crystal Structure (fix) or Relaxed by MM (free)

	N_1	N_2	S_{Cys}	S_{Met}
Reduced State				
QM	2.06	2.05	2.30	2.34
QM/MM, fix	2.06	2.00	2.23	3.13
QM/MM, free	2.09	2.01	2.24	2.96
Oxidized State				
QM	2.03	2.09	2.21	2.40
QM/MM, fix	1.99	1.99	2.18	2.98
QM/MM, free	2.00	2.01	2.19	2.81

We can also use the QM/MM-2QM structures to calculate the difference in redox potentials of the two copper sites. With mechanical embedding (ME), the QM energies are directly comparable to the vacuum QM energies and reflect the effect of the difference in geometry of the Cu sites in vacuum and in the protein. From Table 1, it can be seen that the redox potentials of both sites change if the QM/MM-2QM geometries are used: The potential of the T1 site decreases by 0.2 V, probably reflecting a shortening of the Cu−N_{His} and Cu−S_{Cys} bonds by 0.03−0.10 Å in the oxidized state, but by only 0.01−0.07 Å in the reduced state (Table 2). At the same time, the Cu−S_{Met} bond length increases by 0.4−0.8 Å, but it has a negligible influence on the energies.[92,93] For the T23 site, the potential decreases by 0.2−0.4 V. In this case, there are more and larger differences in the geometries of this complicated trinuclear copper cluster (Table 3), but it is hard to decide which of the differences are most important.

When the influence of the surrounding protein and solvent is included in the calculation (the MM term in Table 1), the potentials change by 3.2−3.4 V, reflecting the strong solvation effects of these charged metal sites, confirming the large effect of the solvent in the COSMO QM calculations. Therefore, the ME calculations predict that the OR state is 72 (fixed protein) or 106 kJ/mol (relaxed protein) more stable than the RO state in the protein.

With EE, the QM energies are no longer comparable with the vacuum energies, but we can instead see how the electrostatic solvation energy affects the two metal sites. It can be seen that the oxidized state of the T1 site is strongly favored in the protein (the redox potential is −2.6 V). The same also applies for the oxidized state of the T23 state (the PI), giving a redox potential of −2.2 to −3.0 V in the protein. In both cases, the effect is appreciably larger than what is predicted for the two sites in water solution. However, the stronger effect in the relaxed protein is counteracted by a MM term of a similar size but an opposite sign, so that the net effect in the protein is that the OR state is still predicted to be more stable by 36−41 kJ/mol. Thus, we see a larger effect of the surrounding protein in the EE calculations as expected.

We have also calculated the redox potential difference with the QM/MM-PBSA approach (using a vacuum wave function).[75] The results of these calculations are also included in Table 1, and

Table 3. Cu−Cu and Cu−Ligand Distances of the T23 Cu Cluster Obtained in the QM and QM/MM-2QM Calculations with the Surrounding Fixed at the Crystal Structure (fix) or Relaxed by MM (free)

	Cu_1							Cu_2						Cu_3				
	N_1	N_2	Cu_2	Cu_3	O_1	O_2	O_{Wat}	N_3	N_4	N_5	Cu_3	O_1	O_2	N_6	N_7	N_8	O_1	O_2
Reduced State = Native Intermediate																		
QM	1.97	1.97	2.75	4.59	2.03	2.93	4.32	2.08	2.04	2.09	4.47	2.03	2.96	2.07	2.05	2.08	2.85	1.98
QM/MM, fix	1.92	1.93	3.49	4.03	2.09	3.03	2.61	2.02	2.09	2.03	4.39	1.98	2.63	1.99	1.99	2.05	2.83	1.97
QM/MM, free	1.93	1.94	3.35	4.07	2.08	2.94	3.36	2.05	2.11	2.04	4.52	2.01	2.73	2.03	2.03	2.08	2.86	1.99
Oxidized State = Peroxy Intermediate																		
QM	1.94	1.94	3.68	4.25	2.06	3.00	3.93	2.04	2.04	2.13	3.94	2.01	2.18	2.03	2.06	2.07	2.91	1.99
QM/MM, fix	1.93	1.94	3.64	4.18	2.19	3.11	2.39	2.02	2.07	2.02	4.40	2.01	2.59	2.01	1.98	2.04	2.88	1.99
QM/MM, free	1.94	1.94	3.67	4.16	2.22	3.09	2.68	2.04	2.07	2.03	4.50	2.03	2.66	2.04	2.02	2.06	2.91	2.00

Table 4. Reorganization Energies (kJ/mol), Calculated by QM or QM/MM-2QM, the Latter with Either Mechanical (ME) or Electrostatic Embedding (EE) and with the Surroundings Either Fixed (fix) or Free to Relax[a]

	T1		T23		MM contribution		total	
	Red	Ox	Red	Ox	RO	OR	RO	OR
QM, PBE/B1	35.8	21.3	31.2	29.7			65.5	52.5
QM, PBE/B2//PBE/B1	28.8	24.3	17.7	54.5			83.3	42.0
QM, PBE/B2	30.6	19.0	28.2	40.9			71.5	47.2
QM, B3LYP/B1//PBE/B1	34.4	25.0	15.6	34.1			68.5	40.6
QM, B3LYP/B1	34.6	21.9	28.8	43.7			78.3	50.7
QM, B3LYP/B2//PBE/B1	26.0	36.7	−10.3	75.9			101.9	26.4
QM, B3LYP/B2	27.0	21.2						
ME, fix	9.6	5.7	16.6	13.6	−13.8	23.9	9.4	46.2
ME, free	9.7	5.8	24.9	15.3	32.2	78.3	57.2	109.0
EE, fix, it1	14.2	10.1	19.5	16.7	−1.9	1.9	28.9	31.5
EE, fix, it2	15.4	8.6	17.8	13.8	−1.9	1.9	27.4	28.3
EE, fix, it3	15.4	8.6	17.9	13.9	−1.9	1.9	27.4	28.4
EE, free, it1	18.7	56.5	−69.8	161.1	−77.0	77.0	102.8	63.6
EE, free, it2	20.0	54.9	−71.3	158.6	−77.0	77.0	101.7	60.6
EE, free, it3	20.0	54.9	−71.2	158.7	−77.0	77.0	101.8	60.7

[a] The EE calculations are done iteratively because the ESP charges of one QM system affect the wavefunction of the other QM system.

it can be seen that this method is also based on ME so that the QM energies are identical to those obtained with ME. However, QM/MM-PBSA includes a continuum-solvation (Poisson−Boltzmann) estimate of the water contribution to the redox potential, after stripping off the explicit water molecules. It can be seen that the continuum solvent stabilizes the OR state so that it is slightly more stable than with ME, that is, 112−121 kJ/mol more stable than the RO state.

Finally, we have calculated the energy difference of the two states using the QTCP method. It is also based on the QM/MM-2QM structures (with a fixed surrounding), but it uses a larger and better solvated system, and it employs MD simulations of the protein and the solvent (keeping the two QM system fixed) and free-energy perturbations, both between the two redox states and between a MM and QM/MM description.[68,69] Simulations were performed using both the RO and the OR QM/MM structures, and they gave similar results: In both cases, the OR state was found to be more stable by (43−46) ± 2 kJ/mol. This energy is dominated by the QM energy, ∼407 kJ/mol, that is, close to the raw QM (ME) results for the QM/MM-2QM structure (the 5 kJ/mol difference comes from the MM → QM/MM correction). This energy is counteracted by a solvation energy from the change in the charge distribution in the protein, 359−368 kJ/mol. The term coming from the change in geometry of the two Cu sites upon electron transfer is only 2 kJ/mol. Thus, these results indicate that the effect of protein sampling (which is missing in the QM/MM-PBSA approach) is large and favors the RO state. It is also possible that the difference between these two methods is caused by long-range solvation effects outside the explicitly simulated system in QTCP (which are treated by a simple Onsager model in QTCP). However, the effect of increasing the shell of solvating water molecules by 5 Å in the QTCP calculations (in total 19 803 water molecules) is less than 2 kJ/mol, that is, within the statistical uncertainty. On the other hand, the difference between the EE (used in QTCP) and ME (used in QM/MM-PBSA) approaches is large, up to 65 kJ/mol according to the QM/MM results. This difference reflects the polarization of the QM system, but also errors caused by the introduction of HL atoms in the QM/MM treatment.

Reorganization Energies of Minimized Structures. We can also use the QM and QM/MM-2QM structures to calculate REs

using eq 2. The results are collected in Table 4. The isolated T1 site gives an inner-sphere REs of 36 kJ/mol for the reduced state and 21 kJ/mol for the oxidized state at the PBE/def2-SVP level, which is similar to what was obtained at the B3LYP/6-31G* level before (33 and 29 kJ/mol).[11] The isolated T23 site gives similar inner-sphere RE, 30−31 kJ/mol, for the two oxidation states. Therefore, the QM calculations indicate that the inner-sphere RE for the RO state is 66 kJ/mol and that of the OR state is 52 kJ/mol.

The REs are rather insensitive to the DFT functional and basis set. With the B3LYP and the def2-TZVP basis set, the reduced T1 site gives a smaller RE (27 kJ/mol), but the oxidized T23 site gives a larger RE (44 kJ/mol). It can also be seen that single-point calculations on structures optimized by other methods give inaccurate and quite erratic results. Thus, such an approach, which has been frequently used before,[15,25] is not recommended.

If instead the QM/MM-2QM minimized structures are used, we can still estimate the inner-sphere contribution to the RE using the ME calculations. It is 10 and 6 kJ/mol for the two oxidation states of the T1 site and 17 and 14 kJ/mol for the two oxidation states of the T23 site with ME and a fixed protein. This is 2−4 times smaller than the REs observed for the isolated systems, in accordance with our previous observations for blue-copper proteins and iron−sulfur clusters.[12,14] The inner-sphere REs for the T1 site hardly change if the protein is allowed to relax, but those of the T23 site increase by 2−8 kJ/mol.

The outer-sphere contribution can be estimated in a similar manner, but this approximation is more questionable for this contribution, because only parts of the surroundings are relaxed in the QM/MM-2QM minimization and only minimized structures are used. With ME and a fixed protein, the calculated outer-sphere RE (i.e., the MM contribution) is 24 kJ/mol for the RO state, which reflects the effect of the changed charge and electron distribution in the two active sites on a fixed protein structure. However, the RE is actually negative for the RO state, indicating that the fixed structure is better for the OR structure than for the RO structure for this state. However, if the protein is allowed to relax, this contribution becomes positive as expected (32 kJ/mol), which reflects also the effect of structural relaxations of the surrounding protein (but still only residues within 6 Å of the two copper sites). The outer-sphere RE of the OR state increases to 78 kJ/mol. This is probably a more realistic measure, but it corresponds to a single minimized structure, that is, a single local minimum among very many possible, and the relaxation of the rest of the protein and the solvent is still ignored.

Finally, we calculated the RE also with EE. As was discussed in the Methods, EE is often considered to be more accurate than ME, but ME avoids several problems with EE (HL atoms at wrong positions and with wrong charges, as well as overpolarization the two QM system).[64] Moreover, in these calculations with two separate QM systems, the point-charge model of one QM system depends on the other QM system, so that the calculations need to be run in an iterative manner (reasonably stable energies were obtained after three iterations, as can be seen from the results in Table 2). The total RE is 27 and 28 kJ/mol with a fixed protein and 102 and 61 kJ/mol when the protein was allowed to relax, for the RO and OR states, respectively. Thus, there is little consensus between the ME and EE calculations.

Parametrization. Next, we wanted to calculate the RE of the IET between a reduced T1 site and the PI state of the T23 cluster using the methods developed by Warshel, Sprik, and Blumberger.[15,16,18,20−22,27] The MD simulations were performed at the MM level. Therefore, force-field parameters of the T1 and T23 centers in the two oxidation states are needed. However, obtaining MM parameters for such complicated metal sites is far from trivial.

Table 5. Performance of the Various Parametrizations of the Four Cu Sites[a]

	T1 ox	T1 red	T23-PI	T23-NI′	PI-Hess2FF
bonds	0.006	0.002	0.002	0.001	0.009
bond *E*	0.026	0.005	0.003	0.002	0.006
angles	0.74	0.66	0.13	0.13	1.10
angle *E*	0.039	0.018	0.019	0.022	0.024
dihedrals	1.68	0.65	0.46	0.42	3.43
dihedral *E*	0.052	0.004	0.071	0.034	0.159
coordinates	0.12	0.06	0.11	0.03	0.46
max coord	0.35	0.17	0.24	0.11	1.01
r^2 Hessian	0.995	0.996	0.996	0.993	0.961

[a] The quality measures are the correlation coefficient (r^2) between all QM and MM Hessian elements, the root-mean-squared deviations (RMSD) for all bonds, angles, dihedral angles, and coordinates between the MM and QM optimized structures (in angstroms or degrees), the maximum deviation (Max) for the coordinates, and the RMSD energy terms (*E*) for the bonds, angles, and dihedral angles (in kJ/mol). Results are shown for the parametrization of the T1 site in the oxidized and reduced states, as well as the T23 cluster in the PI and NI′ states. The last column contains the results for the T23-PI site obtained with the more approximate Hess2FF method.[81]

Several methods exist for the treatment of metal centers by MM,[94] and there are already several sets of parameters for the T1 site.[93,95,96] The simplest approach is a nonbonded model, in which no bonds between the metal and the ligands are defined.[97] However, such a model typically gives rather poor results, and there is a great risk that the ligands may dissociate from the metal and other ligands may bind during the MD simulations.[98] Therefore, it is more common that metal sites are treated by a bonded model, in which the bonds between the metal and its ligands are treated the same way as covalent bonds within the protein, that is, by terms for bonds, angles, and dihedral angles.[99,100]

However, for such a potential, a large number of parameters need to be determined. Several automatic methods have been suggested to obtain what is needed from the Hessian matrix, available from a QM frequency calculation.[81,98,101,102] Unfortunately, such approaches are only approximate, because they assume that the bond lengths, angles, and dihedrals observed in a QM optimized structure are unstrained, which is not correct.[94] Instead, they are a compromise of the preferences of all bonds, angles, and dihedral around the metal, as well as all nonbonded interactions in the complex. Moreover, they involve a double-counting of van der Waals and electrostatic effects within the complex.[94] The automatic methods are fast and appropriate when a robust and reasonable model is needed, for example, when the metal site is not of central interest for the investigation.[94] However, in the present case, it is important that we reproduce the geometries of the metal sites as accurately as possible.

Therefore, we have performed a detailed parametrization of the two metal centers in both oxidation states using the ideal method suggested by Norrby and Liljefors.[64] This approach uses also QM data in the form of optimized structures and the Hessian matrix. However, in this case, it is not assumed that the QM-optimized bonds, angles, and dihedrals are unstrained and double-counting is

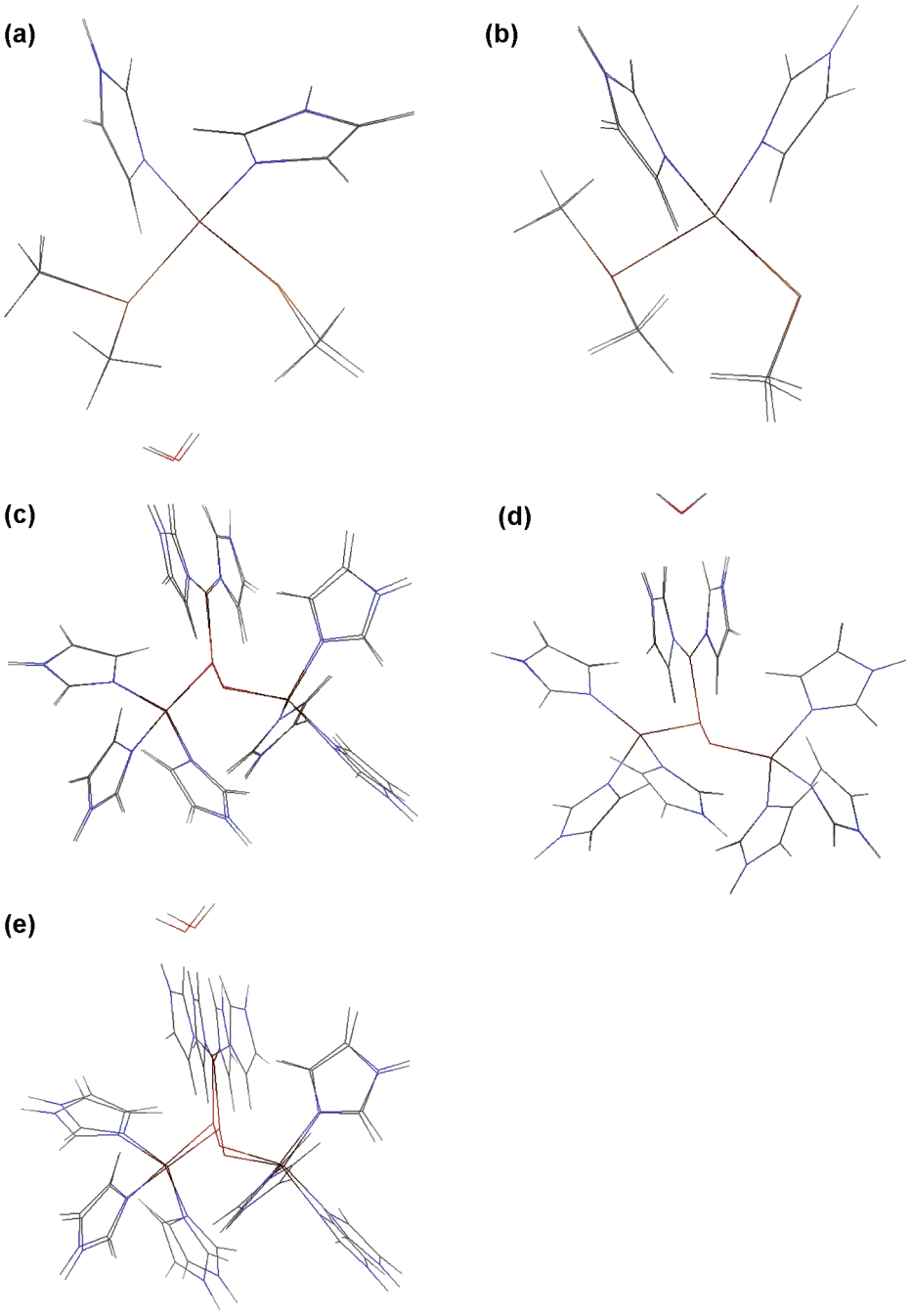

Figure 4. Comparison of the optimized QM and MM structures of the QM models of the four Cu sites: (a) T1-reduced, (b) T1-oxidized, (c) T23-PI, and (d) T23-NI′. In (e), a structure obtained with an automatic Hess2FF approach for T23-PI is shown.

avoided.[94] Instead, all bonded parameters are optimized by an iterative procedure in which a target function is minimized, involving all bonds, angles, dihedrals, and Hessian elements of the complex, performing a full MM geometry optimization and frequency calculation for each sets of parameters. Thereby, it is ensured that the final parameters reproduce the QM structure and Hessian as well as possible. This approach has frequently been used to obtain accurate structures and energies for metal sites.[79,103]

Such a parametrization was performed as is described in the Methods both for the T1 and T23 centers and in both their reduced and oxidized states (the PI and NI′ states for the T23 site). The final force-field parameters are given in the Supporting Information. The performance of the parametrizations is described in Table 5. It can be seen that all four parametrizations perform excellently: They reproduce all bond lengths in the QM structure with a root-mean-squared deviation (rmsd) of less than 0.01 Å, the angles with an rmsd of 0.1−0.7°, the dihedral angles with an rmsd of 0.4−1.7°, and the coordinates with an rmsd of 0.03−0.012 Å and with a maximum difference of 0.11−0.35 Å. Consequently, the rmsd values of the energy are less than 0.1 kJ/mol for all of the bonds, angles, and dihedrals. Moreover, the correlation coefficient between the QM and MM Hessian elements is above 0.993 for all four force fields. This excellent behavior is illustrated by the overlay of the four QM and MM structures in Figure 4. It can be

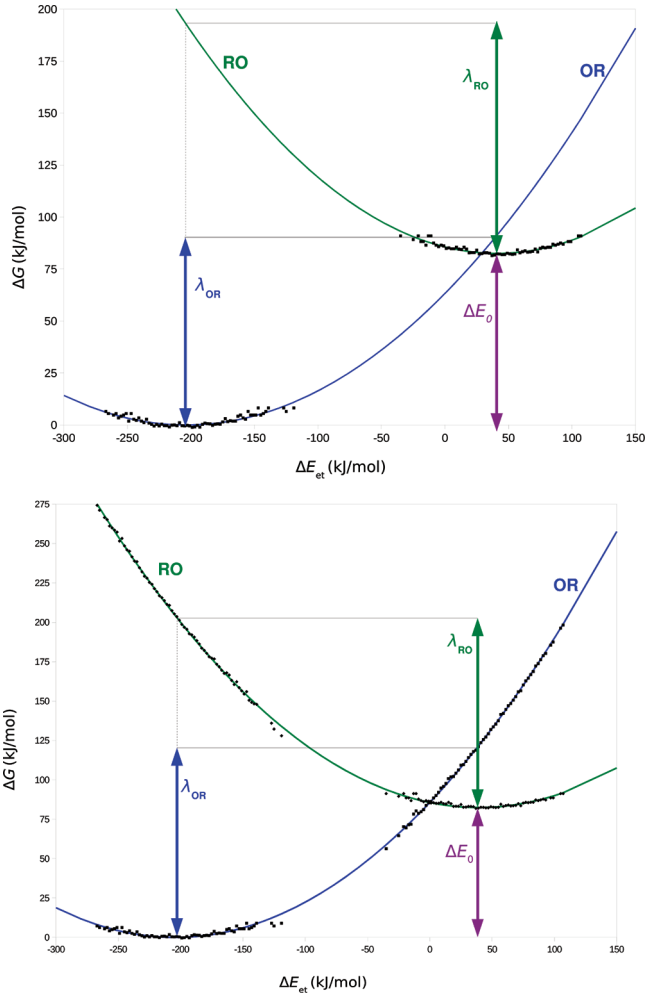

Figure 5. Marcus parabolas for the internal electron transfer in CueO, calculated at the QM/MM-2QM level. The black points are the free energies estimated from eq 8 using the data from the MD simulations. The corresponding parabolas are obtained by nonlinear regression from these data, fitting to a harmonic function, $\Delta G = a(\Delta E_{et} - b)^2 + c$. In (a), only the original low-energy data are used, which gave $\Delta G_{OR} = 0.0015(\Delta E_{et} - 203.7)^2 + 10.9$ and $\Delta G_{RO} = 0.0018(\Delta E_{et} - 41.1)^2 + 10.5$. In (b), also high-energy points are included, generated by eq 11. The problem that $\Delta E_0 = (a_{OR} + a_{RO})/2$ depends on the fit was solved by running the fit iteratively. This gave $\Delta G_{OR} = 0.00205(\Delta E_{et} - 204.3)^2 + 10.1$ and $\Delta G_{RO} = 0.00205(\Delta E_{et} - 39.4)^2 + 10.1$. The REs are estimated from the ΔG value on each curve at the minimum for the OR and the RO curves (i.e., at the b values of the two regression lines). The OR curve has been translated to $\Delta G = 0$ at the minimum, and the RO curve has been translated by the difference in the redox potentials. However, the REs are independent of these translations, because they are measured on a specific curve RO or OR, whereas the translation only affects the value c in the regression line, which cancels when the RE is calculated as the difference $\Delta G(b_{OR})$ and $\Delta G(b_{RO})$.

seen that the fit is best for the NI′ and T1-Red structures, for which only a few dihedral angles of the ligands are not perfectly reproduced. For the T1-oxidized and PI sites, the fits are slightly worse, but still very good.

For comparison, Figure 4e shows the structure obtained with a force field for the T23-PI center using the automatic Hess2FF method.[81] It can be seen that the structure is appreciably worse, with up to 9 times larger deviations in the bonds, angles, dihedrals, and

Table 6. Contributions to the QM/MM REs of CueO, Obtained Using Equation 7[a]

	ME		EE	
	RE	SE	RE	SE
total	122.9	0.8	126.1	2.4
QM T1	12.3	0.3	65.8	2.5
QM T23	22.0	0.3	54.9	2.1
MM	88.7	0.7	5.4	0.9
bonds	0.0	0.0	0.0	0.0
angles	0.1	0.2	−0.1	0.0
dihedrals	0.0	0.0	0.0	0.0
van der Waals	0.3	0.0	5.6	0.9
electrostatics	88.4	0.7	0.0	0.0

[a] All energies are in kJ/mol. SE is the standard error of the RE terms.

coordinates (Table 5). On the other hand, it should be noted that the Hess2FF force field is obtained in seconds (once the QM optimization and frequency calculation have been performed), whereas the parametrization with the method of Norrby and Liljefors took several weeks for the T23 sites. However, when the metal site is of central interest, this effort is needed to obtain reliable energies.

Reorganization Energies from the MD Simulations. Once the metal sites have been parametrized, 10 ns MD simulations (after equilibration) were run for the two oxidation states, RO and OR. The MD trajectories were stable and gave root-mean-squared deviations from the starting crystal structure of 1.29 and 1.30 Å for the backbone atoms of the RO and OR states, respectively. The final densities were 1.03 kg/L for both systems. REs were then extracted using two different methods (eqs 7 and 8) with energies calculated by QM/MM-2QM.

First, we used the approach by Warshel,[16] defining ΔE_{et} as the reaction coordinate and constructing the Marcus parabolas for the IET. The results are shown in Figure 5a. It can be seen that the energies follow parabolas to a reasonable approximation and that the two parabolas have similar curvatures of about 0.0015 (OR) and 0.0018 mol/kJ (RO; the uncertainty in both fits is 0.0001). The exact values depend on how the energies are binned and how the curves are fitted. Taking the difference between the free energies between the minimum for OR and for RO on these fitted curves (see Figure 5a), the REs can be estimated to 91 kJ/mol for the OR curve and 110 kJ/mol for the RO curve at the QM/MM-2QM level. However, it can be seen that these estimates are extrapolations from data points that cover an energy range of only 10 kJ/mol.

The accuracy of the fits can be improved by using the relation:

$$\Delta E_{et} + \Delta E_0 = \Delta G_{OR} - \Delta G_{RO} \quad (11)$$

which follows directly from the linear-response approximation[15,16,22,104] and allows for the generation of twice as many points on the two free energy curves in Figure 5, without doing any new simulations. It also forces the two curves to have the same curvature. This is done in Figure 5b, and now the two parabolas gave much more accurate fitted curvatures, 0.00205 ± 0.000001 mol/kJ. Both curves also gave the same RE, 122 kJ/mol.

Alternatively, the REs can be estimated from eq 7. We then obtain a RE of 123 ± 1 kJ/mol at the QM/MM-2QM level (Table 6). Thus, we see that the two methods give identical results, once the high-energy points are also included. Naturally,

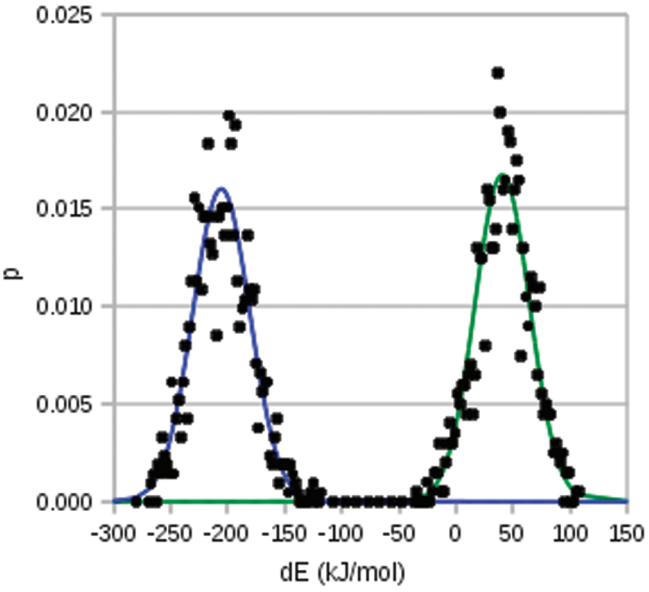

Figure 6. Probability of the various energy gaps (ΔE_{et}) in the simulations of the OR (left) and RO (right) states, calculated at the QM/MM-2QM level (■). The two lines show the Gaussian distributions (eq 12) with the mean value and variances from the simulations ($\mu = -205.5$ and 40.4 kJ/mol, and $\sigma^2 = 618.6$ and 567.0 kJ^2/mol^2 for the OR and RO simulations, respectively). The bin size was 2 kJ/mol.

the two methods are closely related.[3,16,20] Marcus theory assumes that the distribution of the two states is Gaussian with respect to ΔE_{et}, that is, that

$$p(\Delta E_{et}) = \frac{e^{-(\Delta E_{et} - \mu)^2/2\sigma^2}}{\sqrt{(2\pi\sigma^2)}} \quad (12)$$

where p is the probability of observing a certain value of ΔE_{et}. Our simulations show that this is a reasonable assumption, as can be seen in Figure 6. The parameters μ and σ^2 are the average and variance, and they can be estimated directly from the simulations: −206 kJ/mol and 619 (kJ/mol)^2 for the OR simulation, and 40 kJ/mol and 567 (kJ/mol)^2 for the RO simulation. This relation can be inserted into eq 8, which gives Marcus parabola, based on μ and σ^2, thereby avoiding the harmonic curve fit. Using the values of μ and σ^2 from the simulations gives the REs of 122 and 133 kJ/mol, for the OR and RO simulations, respectively. Moreover, the theory requires that the two parabolas have the same curvature, given by $1/2(\mu_{RO} - \mu_{OR}) = 0.0020$,[20] which gives a reorganization energy of 123 kJ/mol. Finally, the reorganization energy can also be calculated directly from $(\sigma^2)/(2RT)$,[15,105] which gives 124 and 114 kJ/mol for the OR and RO simulations, respectively.

Some further understanding of the RE can be obtained by dividing the results from eq 7 into various contributions. From Table 6, it can be seen that the contributions from the two QM systems are 12 kJ/mol for the T1 site and 22 kJ/mol for the T23 cluster. These are estimates of the inner-sphere RE for these two centers, indicating that the inner-sphere contribution is quite small, but not negligible as often is assumed. They are slightly smaller than the inner-sphere REs obtained from the QM/MM structures (Table 2, lines ME, sum of Red and Ox states) and therefore appreciably smaller than the REs calculated for isolated QM clusters, showing that isolated QM calculations give quite misleading results.

Thus, the RE is dominated by the MM part, 89 kJ/mol (which is the sum of the three MM terms in eq 4). This energy can be further divided into contributions from bonds, angles, dihedrals, van der Waals, and electrostatics. From Table 6, it can be seen that the former three terms essentially vanish, and the van der Waals term is also small, less than 1 kJ/mol. Thus, the MM energy is completely dominated by the electrostatic term (88 kJ/mol). The MM term corresponds to the outer-sphere RE.

Further, understanding of the RE can be obtained by dividing the electrostatic interactions into contributions from different residues in the protein and from the solvent. It turns out that 37% of the outer-sphere RE comes from surrounding solvent (34 kJ/mol). It is often assumed or observed that the solvent dominates the outer-sphere RE,[15,18] although this not the case for all proteins.[105] In our case, for which there is no change in the net charge of the protein, the solvent contribution to the RE is rather small. Many residues contribute to the protein term, all providing rather small contributions. The largest contribution is only 8 kJ/mol and comes from Asp-439, which is hydrogen bonded to one of the T1 copper His ligands. The second largest contribution is 4 kJ/mol, from Pro-444, which is next to the same His ligand in sequence and which has a backbone CO group directed toward the T1 Cu at a distance of 5.7 Å. Similar effects have been observed for other proteins.[105]

To check the accuracy of the fixed ESP-charge model of the QM systems, we also tested to calculate the RE by EE. The results of those calculations are also collected in Table 6. It can be seen that RE is almost the same as with ME, 126 ± 2 kJ/mol, indicating that the polarization of the QM system is not very important for the RE (the larger statistical uncertainty of the EE estimates is caused by the fact that fewer snapshots were used for these calculations). The disadvantage with the present implementation of EE is that the RE can no longer be divided into inner- and outer-sphere contributions or to calculate contributions from the various residues and solvent. Instead, all electrostatic interactions between the QM systems and the surroundings are estimated in the QM calculations, whereas the electrostatic MM contribution vanishes (because the charges of the QM systems are zeroed in the MM calculations). The contribution from the T1 Cu site is 66 and 55 kJ/mol from the T23 Cu site, whereas the van der Waals MM contribution is 5 kJ/mol.

Finally, we have also calculated the RE using a bigger basis set (def2-TZVP) or with the B3LYP method (using eq 7 and 125 snapshots). Both changes had only minor effects on the RE: With the bigger basis set, the RE decreased by 1 kJ/mol, but on the other hand, the RE increased by the same amount when the DFT method was changed to B3LYP.

Redox Potentials. Finally, we can also calculate the driving force in the RO → OR reaction, that is, the difference in the redox potentials of the RO and OR states inside the protein, using eq 10, which is the linear-response approximation to a one-step thermodynamic integration estimate of the redox potential.[15,20−22,27] The results in Table 7 show that the ME calculations predict that the OR state is 87 ± 1 kJ/mol more stable than the RO state. Thus, the results indicate that the PI → NI′ step in CueO is exergonic. Interestingly, the contributions (also shown in Table 7) indicate that the redox potential of the T1 site 0.43 V, that is, slightly less positive than in a vacuum, but slightly more positive than with QM/MM-2QM (ME line in Table 1). The redox potential of the T23 copper cluster is 4.70 V, that is, also slightly less positive than in a vacuum, but slightly more positive than in the QM/MM-2QM calculations. The MM energy counteracts the formation of the OR state by 325 kJ/mol. This energy comes almost entirely from electrostatics.

Table 7. Contributions to the QM/MM-2QM Difference in the Reduction Potentials of the RO and OR States, Obtained Using Equation 10 (a Negative Sign Indicates That the OR State Is More Stable)[a]

	ME		EE	
	E0	SE	E0	SE
total	−0.90	0.008	−0.74	0.03
QM T1	0.43	0.003	−1.47	0.03
QM T23	4.70	0.003	−0.55	0.02
MM	3.37	0.007	0.11	0.01
bonds	0.00	0.000	0.00	0.00
angles	0.00	0.002	0.00	0.00
dihedrals	0.00	0.000	0.00	0.00
van der Waals	0.00	0.000	0.12	0.01
electrostatics	3.37	0.007	0.00	0.00

[a] All energies are in eV and are obtained with eq 10. SE is the standard error of the RE terms. To the total and QM energies has been added the zero-point energy, obtained from a frequency calculation of the isolated QM systems at the PBE/def2-SV(P) level (0.07 eV for the T1 site and 0.11 eV for the T23 Cu cluster).

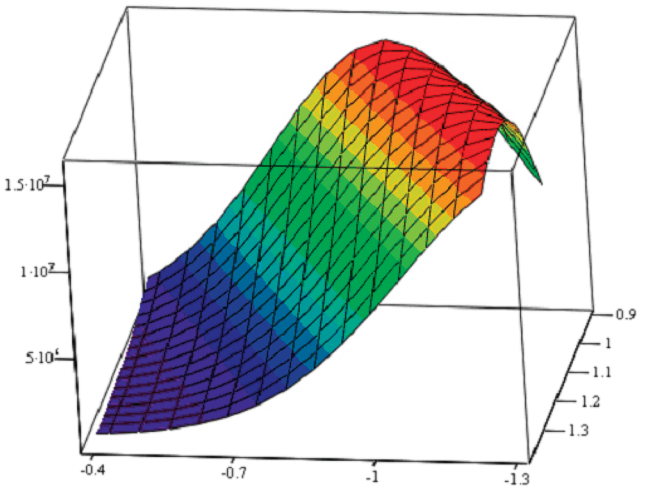

Figure 7. The dependence of k_{et} (s^{-1}) on reorganization energies (eV) and energy difference (eV) between the two electronic states involved in the internal electron transfer between the reduced T1 site and the PI of the T23 copper cluster using eq 13.

The large and positive MM energy is understandable if it is considered as a solvation energy: The T1 site goes from a net charge of 0 to +1, that is, a gain in solvation energy, but this is more than compensated by the T23 cluster, which goes from a net charge of +3 to +2.

The net MM energy comes almost entirely from the solvent; the net effect of the protein residues is only 4 kJ/mol. However, this is mainly because the protein contributions cancel; the individual contributions from the protein residues are up to 131 kJ/mol for Asp-112. This residue forms three hydrogen bonds to two of the T23 copper ligands. Other large contributions come from Asp-439 (−122 kJ/mol), Asp-471 (95 kJ/mol), and Arg-280 (−66 kJ/mol). Asp-471 also forms hydrogen bonds to two of the T23 copper ligands, whereas Arg-280 is close to the T23 cluster and forms two hydrogen bonds to Asp-471.

With EE, the energy difference between the two states has decreased to 67 ± 2 kJ/mol, which shows that polarization effects are quite significant for the relative stability of the two states. With the def2-TZVP basis set, the energy difference between the RO and OR states decreased by 8 kJ/mol, but with the B3LYP method, it increased by 18 kJ/mol. The individual components from the T1 and T23 centers are in reasonable agreement (within 14 kJ/mol) with those obtained from the optimized structures in a vacuum, shown in Table 1. The standard errors of the extrapolations are less than 1 kJ/mol.

It is somewhat disappointing that the calculations based on eq 10 give quite different relative energies of the RO and OR states as compared to QTCP (43−46 kJ/mol), although both approaches are based on MD simulations. The difference is not caused by the linear-response approximation (used in eq 10, but not in QTCP), because the QTCP results show that this approximation changes the results by only 1−3 kJ/mol. The effect of ESP charges for the QM systems taken from different snapshots is also rather small, 0−6 kJ/mol. The QM energies differ by only 5 kJ/mol (after addition of thermal and zero-point energy corrections). Approximately 10 kJ/mol of the difference comes from differences in the treatment of the long-range electrostatic effects (i.e., the solvation outside the ∼55 Å radius of the explicitly simulated system; the MD simulations use particle mesh Ewald summation, whereas the QTCP calculations use the Onsager relation; no long-range treatment at all gives a difference of ∼20 kJ/mol as compared to Ewald summation). The rest of the difference comes from differences in the simulated structures (i.e., from the geometries in the sampled snapshots). This may indicate that the MM force field of the Cu centers is not accurate enough to extract reliable QM energy differences. On the other hand, the Cu sites have fixed geometries in the QTCP calculations, which also is a somewhat questionable approximation.

Rate of IET. Finally, we can check if our computational results are reasonable by estimating the rate constant (k_{et}) for the IET between the reduced T1 site and the PI of the T23 copper cluster using a simple empirical expression that incorporates an exponential decay of the tunneling rate with the distance between the two redox-active sites (R in Å) and a parabolic dependence on energy difference (ΔG) and RE (λ), both in eV:[36]

$$\log(k_{et}) = 15 - 0.6R - 3.1[(\Delta G + \lambda)^2/\lambda] \quad (13)$$

Using R = 13 Å, the approximate distance between the T1 site and T23 cluster,[29] as well as the REs (0.94−1.38 eV) and free-energy differences (−0.37 to −1.25 eV) calculated in the present work, k_{et} falls in the range from 8×10^4 to 2×10^7 s^{-1} (Figure 7). These approximate results are compatible with the experimentally observed k_{et} value for this IET step (>1000 s^{-1}) measured for a low-potential laccase,[86] a MCO with the same set of ligands as used in our calculations. Thus, taking into account experimentally observed maximal turnover rates of MCOs toward different substrates, which is below 600 s^{-1},[29,35,86] one can conclude that both theoretically calculated and experimental k_{et} values point to the fact that the IET between the T1 site and PI of the T23 cluster is not the rate-limiting step in the overall catalytic cycle of these enzymes.

CONCLUSIONS

In this investigation, we have made a detailed study of the reorganization energy for the intramolecular electron transfer between the peroxy intermediate and the reduced T1 copper site

in the multicopper oxidase CueO. We have employed the methods developed by Warshel, Sprik, and co-workers,[15,16,20] based on MD simulations of protein, using accurate force-field parametrizations of the two Cu centers in both their oxidized and their reduced states obtained by the ideal method of Norrby and Liljefors,[78] which has been shown to be appreciably more accurate than other methods to parametrize metal sites in proteins.[94,103]

The results indicate that the RE is 91−133 kJ/mol (0.94−1.38 eV), depending on the methods used and the assumptions engaged. On the other hand, the estimates do not seem to be sensitive to the DFT method and basis sets used in the calculations, although this may be partly fortuitous, considering the rather large effects (up to 14 kJ/mol) observed for the isolated systems in a vacuum in Table 2. The RE is also rather insensitive to details in the QM/MM-2QM calculations. The inner-sphere contributions from the T1 and T23 centers are 12 and 22 kJ/mol, respectively. The outer-sphere contribution (89 kJ/mol) comes entirely from electrostatic interactions, approximately one-third from the solvent and the rest from the protein. The protein contribution is the sum of many small contributions from different residues; the two largest (8 and 4 kJ/mol) come from Asp-386 and Pro-391, close to the T1 Cu site. The unusually low RE from the solvent[15,105] can be attributed to the fact that an intraprotein electron transfer is studied, in which the net charge of the protein is not changed. Furthermore, the T1 and T23 copper sites are in the protein interior, and therefore the electron transfer is less susceptible to solvent effects.

We have also estimated the RE from QM/MM minimized structures. These are much more varying and depend quite strongly on the details of the calculations, but in general they are 10−30 kJ/mol lower than the estimates based on MD simulations. This difference most likely comes from the solvent, which is not fully relaxed in the QM/MM calculations. On the other hand, the inner-sphere REs estimated from vacuum structures are too large by 10−20 kJ/mol.

The calculations also allowed us to estimate the energy difference between the two electronic states involved in the electron transfer, RO and OR. The calculations indicate that the OR state is more stable, that is, that the reduction of the peroxy intermediate by the reduced T1 site is exergonic. The energy difference from the MD simulations is 87 kJ/mol, and it is strongly affected by the surroundings. The net effect of the protein is small, 4 kJ/mol, but this is the effect of many large residue contributions with differing sign, up to 131, −122, and 95 kJ/mol for Asp-82, Asp-386, and Asp-418, residues hydrogen-bonded to the His ligands of the two Cu centers. This energy difference is sensitive to the details of the calculations, changing by up to 20 kJ/mol in either direction if the DFT method or basis set is changed, or if the EE is used in the QM/MM calculations. Even worse, the QTCP method, which also is based on QM/MM-2QM calculations and MD simulations (but with a fixed QM system), gives a much smaller energy difference, 43−46 kJ/mol. It remains to be demonstrated which of the two approaches is more accurate.

Finally, the rate constant for the IET between the T1 site and PI of the T23 copper cluster was estimated, based on the obtained values of REs and energy differences between the two electronic states. The result was in the range from 8×10^4 to 2×10^7 s^{-1}, that is, in good agreement with the experimentally observed rate of this IET step in MCOs (>1000 s^{-1}).

In conclusion, these calculations show that detailed atomistic information can be obtained for the reorganization energies and redox potentials of complex metalloproteins with theoretical methods, although the accuracy is limited. For the small T1 Cu protein azurin, REs of 68−99 kJ/mol have been measured for the electron transfer from the Cu site to a Ru label on the surface of the protein.[5−7] Moreover, the T1 sites have been studied with theoretical methods,[26,106] giving REs of 42−54 kJ/mol for plastocyanin−cytochrome *f* complexes with docked geometries (only outer-sphere contribution) and 70−90 kJ/mol for the reduction of T1 sites in four different MCOs, including CueO (from 10 ps QM/MM MD simulations). Our calculated RE is similar to what has been obtained for the intramolecular electron transfer in Ru-modified cytochromes (96−125 kJ/mol).[15,105] On the other hand, it is somewhat larger than what has been calculated for cytochromes and iron−sulfur proteins metalloproteins (38−75 kJ/mol for the oxidation of the isolated cofactor)[27,107,108] and appreciably larger than what has been obtained for intramolecular electron transfer in cytochrome *c* oxidase and the photosynthetic reaction center (7−32 kJ/mol).[18,25] This is partly due to the larger inner-sphere RE for copper sites than for cytochromes, and partly to the presence of many charged groups around the Cu sites, needed to neutralize the large positive charge of the trinuclear T23 cluster with its neutral His ligands. Moreover, it is likely that our calculations with a nonpolarizable force field may overestimate the RE by ∼35%[15,105,109] (i.e., that simulations in a polarizable force field would give a RE around 75 kJ/mol). However, we have seen that the RE is not too large to support a satisfactory reaction rate of the MCOs.[35]

■ ASSOCIATED CONTENT

Supporting Information. Force-field topology (in) and parameter (dat) files in Amber format for the four copper centers. This material is available free of charge via the Internet at http://pubs.acs.org.

■ AUTHOR INFORMATION

Corresponding Author

*Tel.: +46-46 2224502. Fax: +46-46 2228648. E-mail: ulf.ryde@teokem.lu.se.

■ ACKNOWLEDGMENT

This investigation has been supported by grants from the Swedish research council (projects 2010-5025 and 2009-3266), MSMT CR (project LC512), and the Wenner−Gren foundation. It has also been supported by computer resources of Lunarc at Lund University.

■ REFERENCES

(1) Edwards, P. P.; Gray, H. B.; Lodge, M. T. J.; Williams, R. P. J. *Angew. Chem., Int. Ed.* **2008**, *47*, 6758–6765.

(2) Gray, H. B.; Winkler, J. R. *Proc. Natl. Acad. Sci. U.S.A.* **2005**, *102*, 3534–3539.

(3) Marcus, R. A.; Sutin, N. *Biochim. Biophys. Acta* **1985**, *811*, 265.

(4) Moser, C. C.; Page, C. C.; Dutton, P. L. *Philos. Trans. R. Soc., B* **2006**, *261*, 1295.

(5) Farver, O.; Skov, L. K.; Gilardi, G.; van Puderoyen, G.; Canters, G. W.; Wheland, S.; Pecht, I. *Chem. Phys.* **1996**, *204*, 271–277.

(6) Di Bilio, A. J.; Hill, M. G.; Bonander, N.; Karlsson, B. G.; Villahermosa, R. M.; Malmström, B. G.; Winkler, J. R.; Gray, H. B. *J. Am. Chem. Soc.* **1997**, *119*, 9921–9922.

(7) Winkler, J. R.; Wittung-Stafshede, P.; Leckner, J.; Malmström, B. G.; Gray, H. B. *Proc. Natl. Acad. Sci. U.S.A.* **1997**, *94*, 4246–4249.

(8) Mines, G. A.; Bjerrum, M. J.; Hill, M. G.; Casimiro, D. R.; Chang, I.-J.; Winkler, J. R.; Gray, H. B. *J. Am. Chem. Soc.* **1996**, *118*, 1961.
(9) Haffa, A. L. M.; Lin, S.; Katilius, E.; Williams, J. C.; Taguchi, A. K. W.; Allen, J. P.; Woodubury, N. W. *J. Phys. Chem. B* **2002**, *106*, 7376.
(10) Kuila, D.; Baxter, W. W.; Natan, M. J.; Hoffman, B. M. *J. Phys. Chem. B* **1991**, *95*, 1.
(11) Olsson, M. H. M.; Ryde, U.; Roos, B. O. *Protein Sci.* **1998**, *7*, 2659–2668.
(12) Sigfridsson, E.; Olsson, M. H. M.; Ryde, U. *Inorg. Chem.* **2001**, *40*, 2509–2519.
(13) Sigfridsson, E.; Olsson, M. H. M.; Ryde, U. *J. Phys. Chem. B* **2001**, *105*, 5546–5552.
(14) Ryde, U.; Olsson, M. H. M. *Int. J. Quantum Chem.* **2001**, *81*, 335–347.
(15) Blumberger, J. *Phys. Chem. Chem. Phys.* **2008**, *10*, 5651–5657.
(16) Warshel, A. *J. Phys. Chem.* **1982**, *86*, 2218–2224.
(17) Warshel, A.; Parson, W. W. *Annu. Rev. Phys. Chem.* **1991**, *42*, 279–309.
(18) Parson, W. W.; Chu, Z. T.; Warshel, A. *Biophys. J.* **1998**, *74*, 182–191.
(19) Zhou, H.-X.; Szabo, A. *J. Chem. Phys.* **1995**, *103*, 3481–3494.
(20) Tateyama, Y.; Blumberger, J.; Sprik, M.; Tavernelli, I. *J. Chem. Phys.* **2005**, *122*, 234505.
(21) Blumberger, J.; Tavernelli, I.; Klein, M. L.; Sprik, M. *J. Chem. Phys.* **2006**, *124*, 034507.
(22) Blumberger, J.; Sprik, M. *Theor. Chem. Acc.* **2006**, *115*, 113–126.
(23) Zeng, X.; Hu, H.; Hu, X.; Cohen, A. J.; Yang, W. *J. Chem. Phys.* **2008**, *128*, 124510.
(24) LeBard, D. N.; Matyushov, D. V. *J. Phys. Chem. B* **2009**, *113*, 12424–12437.
(25) Kaila, V. R. I.; Johansson, M. P.; Sundholm, D.; Wikström, M. *Proc. Natl. Acad. Sci. U.S.A.* **2010**, *107*, 21470–21475.
(26) Hong, G.; Ivnitski, D. M.; Johnson, G. R.; Atanassov, P.; Pachter, R. *J. Am. Chem. Soc.* **2011**, *133*, 4802–4809.
(27) Sulpizi, M.; Raugei, S.; VandeVondele, J.; Carloni, P.; Sprik, M. *J. Phys. Chem. B* **2007**, *111*, 3969–3976.
(28) Olsson, M. H. M.; Hong, G.; Warshel, A. *J. Am. Chem. Soc.* **2003**, *125*, 5025.
(29) Solomon, E. I.; Sundaram, U. M.; Machonkin, T. E. *Chem. Rev.* **1996**, *96*, 2563–2605.
(30) Solomon, E. I.; Augustine, A. J.; Yoon, J. *Dalton Trans.* **2008**, 3921–3932.
(31) Messerschmidt, A.; Ladenstein, R.; Huber, R.; Bolognesi, M.; Avigliano, L.; Petruzzelli, R.; Rossi, A.; Finazzi-Agro, A. *J. Mol. Biol.* **1992**, *224*, 179–205.
(32) Roberts, S. A.; Weichsel, A.; Grass, G.; Thakali, K.; Hazzard, J. T.; Tollin, G.; Rensing, C.; Montfort, W. R. *Proc. Natl. Acad. Sci. U.S.A.* **2002**, *99*, 2766–2771.
(33) Ramirez, P.; Mano, N.; Andreu, R.; Ruzgas, T.; Heller, A.; Gorton, L.; Shleev, S. *Biochim. Biophys. Acta* **2008**, *1777*, 1364–1369.
(34) Shleev, S.; Ruzgas, T. *Angew. Chem., Int. Ed.* **2008**, *47*, 7270–7274.
(35) Shleev, S.; Reimann, C.; Andoralov, V.; Falk, M.; Ruzgas, T.; Srnec, M.; Ryde, U.; Rulíšek, L. *FEBS J.*, submitted.
(36) Page, C. C.; Moser, C. C.; Chen, X.; Dutton, P. L. *Nature* **1999**, *402*, 47–52.
(37) Rulíšek, L.; Solomon, E. I.; Ryde, U. *Inorg. Chem.* **2005**, *44*, 5612–5628.
(38) Chalupský, J.; Neese, F.; Solomon, E. I.; Ryde, U.; Rulíšek, L. *Inorg. Chem.* **2006**, *45*, 11051–11059.
(39) Ryde, U.; Hsiao, Y.-W.; Rulíšek, L.; Solomon, E. I. *J. Am. Chem. Soc.* **2007**, *129*, 726–727.
(40) Vancoillie, S.; Chalupský, J.; Ryde, U.; Solomon, E. I.; Pierloot, K.; Neese, F.; Rulíšek, L. *J. Phys. Chem. B* **2010**, *114*, 7692–7702.
(41) Srnec, M.; Ryde, U.; Rulíšek, L. *Faraday Discuss.* **2011**, *148*, 41–53.
(42) Case, D. A.; Darden, T. A.; Cheatham, T. E.; Simmerling, C. L.; Wang, J.; Duke, R. E.; Luo, R.; Crowley, M.; Walker, R. C.; Zhang, W.; et al. *AMBER 10*; University of California: San Francisco, CA, 2008.
(43) Cornell, W. D.; Cieplak, P.; Bayly, C. I.; Gould, I. R.; Merz, K. M.; Ferguson, D. M.; Spellmeyer, D. C.; Fox, T.; Caldwell, J. W.; Kollman, P. A. *J. Am. Chem. Soc.* **1995**, *117*, 5179–5197.
(44) Wang, J.; Cieplak, P.; Kollman, P. A. *J. Comput. Chem.* **2000**, *21*, 1049–1074.
(45) Ryckaert, J. P.; Ciccotti, G.; Berendsen, H. J. C. *J. Comput. Phys.* **1977**, *23*, 327–341.
(46) Darden, T.; York, D.; Pedersen, L. *J. Chem. Phys.* **1993**, *98*, 10089–10092.
(47) Essmann, U.; Perera, L.; Berkowitz, M. L.; Darden, T.; Lee, H.; Pedersen, L. G. *J. Chem. Phys.* **1995**, *103*, 8577–8592.
(48) Berendsen, H. J. C.; Postma, J. P. M.; van Gunsteren, W. F.; DiNola, A.; Haak, J. R. *J. Chem. Phys.* **1984**, *81*, 3684–3690.
(49) Jorgensen, W. L.; Chandrasekhar, J.; Madura, J. D.; Impley, R. W.; Klein, M. L. *J. Chem. Phys.* **1983**, *79*, 926–935.
(50) Perdew, J. P.; Burke, K.; Ernzerhof, M. *Phys. Rev. Lett.* **1996**, *77*, 3865–3868.
(51) Weigend, F.; Ahlrichs, R. *Phys. Chem. Chem. Phys.* **2005**, *7*, 3297–3305.
(52) Eichkorn, K.; Treutler, O.; Öhm, H.; Häser, M.; Ahlrichs, R. *Chem. Phys. Lett.* **1995**, *240*, 283–290.
(53) Eichkorn, K.; Weigend, F.; Treutler, O.; Ahlrichs, R. *Theor. Chem. Acc.* **1997**, *97*, 119–126.
(54) Jensen, F. *Introduction to Computational Chemistry*; J. Wiley & Sons: Chichester, 2007.
(55) Lee, C.; Yang, W.; Parr, R. G. *Phys. Rev. B* **1988**, *37*, 785.
(56) Becke, A. D. *J. Chem. Phys.* **1993**, *98*, 5648.
(57) Treutler, O.; Ahlrichs, R. *J. Chem. Phys.* **1995**, *102*, 346–354.
(58) Shin, W.; Sundaram, U. M.; Cole, J. L.; Zhang, H. H.; Hedman, B.; Hodgson, K. O.; Solomon, E. I. *J. Am. Chem. Soc.* **1996**, *118*, 3202–3215.
(59) Klamt, A.; Schüürmann, G. *J. Chem. Soc., Perkin Trans. 2* **1993**, *5*, 799–805.
(60) Schäfer, A.; Klamt, A.; Sattel, D.; Lohrenz, J. C. W.; Eckert, F. *Phys. Chem. Chem. Phys.* **2000**, *2*, 2187–2193.
(61) Klamt, A.; Jonas, V.; Bürger, T.; Lohrenz, J. C. W. *J. Phys. Chem.* **1998**, *102*, 5074–5085.
(62) Ryde, U. *J. Comput.-Aided Mol. Des.* **1996**, *10*, 153–164.
(63) Reuter, N.; Dejaegere, A.; Maigret, B.; Karplus, M. *J. Phys. Chem.* **2000**, *104*, 1720–1735.
(64) Hu, L.; Söderhjelm, P.; Ryde, U. *J. Chem. Theory Comput.* **2011**, *7*, 761–777.
(65) Besler, B. H.; Merz, K. M.; Kollman, P. A. *J. Comput. Chem.* **1990**, *11*, 431–439.
(66) Senn, H. M.; Thiel, W. *Angew. Chem., Int. Ed.* **2009**, *48*, 1198–1229.
(67) Tu, Y.; Laaksonen, A. *J. Chem. Phys.* **1999**, *111*, 7519–7525.
(68) Rod, T. H.; Ryde, U. *Phys. Rev. Lett.* **2005**, *94*, 138302.
(69) Rod, T. H.; Ryde, U. *J. Chem. Theory Comput.* **2005**, *1*, 1240–1251.
(70) Kästner, J.; Senn, H. M.; Thiel, S.; Otte, N.; Thiel, W. *J. Chem. Theory Comput.* **2006**, *2*, 452–461.
(71) Kaukonen, M.; Söderhjelm, P.; Heimdal, J.; Ryde, U. *J. Chem. Theory Comput.* **2008**, *4*, 985–1001.
(72) Heimdal, J.; Kaukonen, M.; Srnec, M.; Rulíšek, L.; Ryde, U. *ChemPhysChem* **2011**, *12*, in press, DOI: 10.1002/cphc.201100339.
(73) Kästner, J.; Senn, H. M.; Thiel, S.; Otte, N.; Thiel, W. *J. Chem. Theory Comput.* **2006**, *2*, 452–461.
(74) Yang, W.; Bitetti-Putzer, R.; Karplus, M. *J. Chem. Phys.* **2004**, *120*, 2618–2628.
(75) Kaukonen, M.; Söderhjelm, P.; Heimdal, J.; Ryde, U. *J. Phys. Chem. B* **2008**, *112*, 12537–12548.
(76) Kollman, P. A.; Massova, I.; Reyes, C.; Kuhn, B.; Huo, S.; Chong, L.; Lee, M.; Lee, T.; Duan, Y.; Wang, W.; et al. *Acc. Chem. Res.* **2000**, *33*, 889–897.
(77) Kuhn, B.; Kollman, P. A. *J. Med. Chem.* **2000**, *43*, 3786–3791.
(78) Norrby, P.-O.; Liljefors, T. *J. Comput. Chem.* **1998**, *19*, 1146–1166.
(79) Rydberg, P.; Olsen, L.; Norrby, P.-O.; Ryde, U. *J. Chem. Theory Comput.* **2007**, *3*, 1765–1773.

(80) Norrby, P.-O. *J. Mol. Struct. (THEOCHEM)* **2000**, *506*, 9–16.
(81) Nilsson, K.; Lecerof, D.; Sigfridsson, E.; Ryde, U. *Acta Crystallogr., Sect. D* **2003**, *59*, 274–289.
(82) Bartolotti, L. J.; Pedersen, L. G.; Charifson, P. S. *J. Comput. Chem.* **1991**, *12*, 1125–1128.
(83) Kelly, C. P.; Cramer, C. J.; Truhlar, D. G. *J. Phys. Chem. B* **2006**, *110*, 16066–16081.
(84) Shin, W.; Sundaram, U. M.; Cole, J. L.; Zhang, H. H.; Hedman, B.; Hodgson, K. O.; Solomon, E. I. *J. Am. Chem. Soc.* **1996**, *118*, 3202–3215.
(85) Palmer, A. E.; Lee, S.-K.; Solomon, E. I. *J. Am. Chem. Soc.* **2001**, *123*, 6591–6599.
(86) Lee, S.-K.; George, S. D.; Antholine, W. E.; Hedman, B; Hodgson, K. O.; Solomon, E. I. *J. Am. Chem. Soc.* **2002**, *124*, 6180–6193.
(87) Yoon, J.; Mirica, L. M.; Stack, T. D. P.; Solomon, E. I. *J. Am. Chem. Soc.* **2005**, *127*, 13680–13693.
(88) Yoon, J.; Solomon, E. I. *J. Am. Chem. Soc.* **2007**, *129*, 13127–13136.
(89) Holm, R. H.; Kennepohl, P.; Solomon, E. I. *Chem. Rev.* **1996**, *96*, 2239–2314.
(90) Shleev, S.; Tkac, J.; Christenson, A.; Ruzgas, T.; Yaropolov, A.; Whittaker, J. W.; Gorton, L. *Biosens. Bioelectron.* **2005**, *20*, 2517–2554.
(91) Miura, Y.; Tsujimura, S.; Kurose, S.; Kamitaka, Y.; Kataoka, K.; Sakurai, T.; Kano, K. *Fuel Cells* **2009**, *9*, 70–78.
(92) Ryde, U.; Olsson, M. H. M.; Pierloot, K.; Roos, B. O. *J. Mol. Biol.* **1996**, *261*, 586–596.
(93) De Kerpel, J. O. A.; Ryde, U. *Proteins* **1999**, *36*, 157–174.
(94) Hu, L.; Ryde, U. *J. Chem. Theory Comput.* **2011**, *7*, 2452–2463.
(95) Ullmann, G. M.; Knapp, E. W.; Kostic, N. M. *J. Am. Chem. Soc.* **1997**, *119*, 42.
(96) Remenyi, R.; Comba, P. *J. Inorg. Biochem.* **2001**, *86*, 397.
(97) Stote, R. H.; Karplus, M. *Proteins* **1995**, *23*, 12–31.
(98) Lin, F.; Wang, R. *J. Chem. Theory Comput.* **2010**, *6*, 1852–1870.
(99) Hoops, S. C.; Anderson, K. W.; Merz, K. M. *J. Am. Chem. Soc.* **1991**, *113*, 8262.
(100) Ryde, U. *Proteins* **1995**, *21*, 40–56.
(101) Seminario, J. M. *Int. J. Quantum Chem.* **1996**, *60*, 1271.
(102) Peters, M. B.; Yang, Y.; Wang, B.; Fürsti-Molnár, L.; Weaver, M. N.; Merz, K. M. *J. Chem. Theory Comput.* **2010**, *6*, 2935–2947.
(103) Nilsson Lill, S. O.; Forbes, A.; Donoghue, P.; Verdolino, V.; Wiest, O.; Rydberg, P.; Norrby, P.-O. *Curr. Org. Chem.* **2010**, *14*, 1629–1645.
(104) Tachiya, M. *J. Phys. Chem.* **1989**, *93*, 7050–7052.
(105) Tipmanee, V.; Oberhofer, H.; Park, M.; Kim, K. S.; Blumberger, J. *J. Am. Chem. Soc.* **2010**, *132*, 17032–17040.
(106) Soriano, G. M.; Cramer, W. A.; Krishtalik, L. I. *Biophys. J.* **1997**, *73*, 3265–3276.
(107) Muegge, I.; Qi, P. X.; Wand, J.; Chu, Z. T.; Warshel, A. *J. Phys. Chem. B* **1997**, *101*, 825–836.
(108) Simonson, T. *Proc. Natl. Acad. Sci. U.S.A.* **2002**, *99*, 6544.
(109) Blumberger, J.; Lamoureux, G. *Mol. Phys.* **2008**, *106*, 1597–1911.